Overview of Acoustic Tomography of the Atmosphere

V. E. Ostashev, S. N. Vecherin, and D. K. Wilson
U.S. Army Engineer Research and Development Center

17th Long Range Sound Propagation Symposium, 12-13 June 2018, Lyon, France

Outline

1. Introduction

2. Acoustic tomography of the atmosphere (ATA) at the Boulder Atmospheric Observatory (BAO)

3. Forward and inverse problems in ATA

4. Numerical simulations and experimental results pertinent to the BAO tomography array

5. Other schematics and techniques for ATA

6. Conclusions

7. References

1. Introduction

Tomography is widely used in medicine, industry, and science. It uses different kinds of waves such as x-rays, laser beams, ultrasound, sound, and seismic waves propagating through a medium to obtain an image of the medium. The word *tomography* is derived from Ancient Greek *tomos*, which means "slice“, and *graphō*, which means "to write“.

An example of tomography is a CT scan which is widely used in medicine. CT stands for “computed tomography”. Next two slides show a medical CT scanner and explain its principal of operation.

CT scanner

A CT scanner.

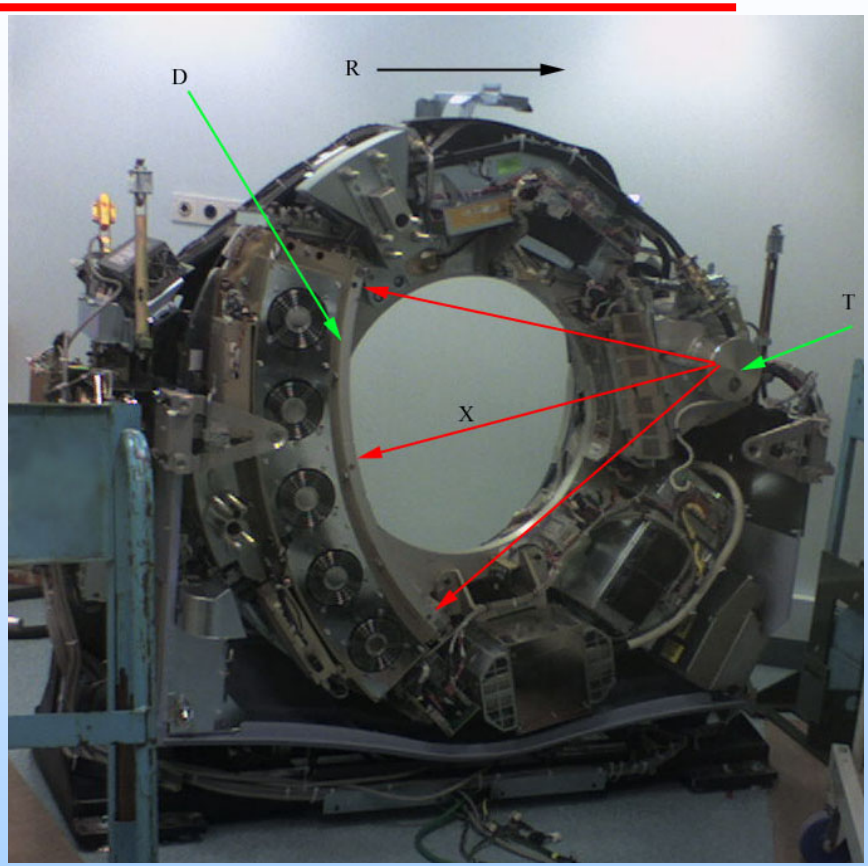

CT scanner with cover removed to show internal components. T: X-ray tube. D: X-ray detectors. X: X-ray beam. R: Gantry rotation

CT scan

Tomography always has two main steps: formulation of a forward problem and a numerical solution of an inverse problem.

1. Forward problem is a formulation of equations describing the effect of a medium on parameters of a propagating wave which are measured experimentally. For a CT scanner, these equations express attenuation of x-rays propagating through a medium with spatially varying properties such as composition and density.

2. Inverse problem is a numerical solution of the equations formulated in the forward problem to infer properties of the medium.

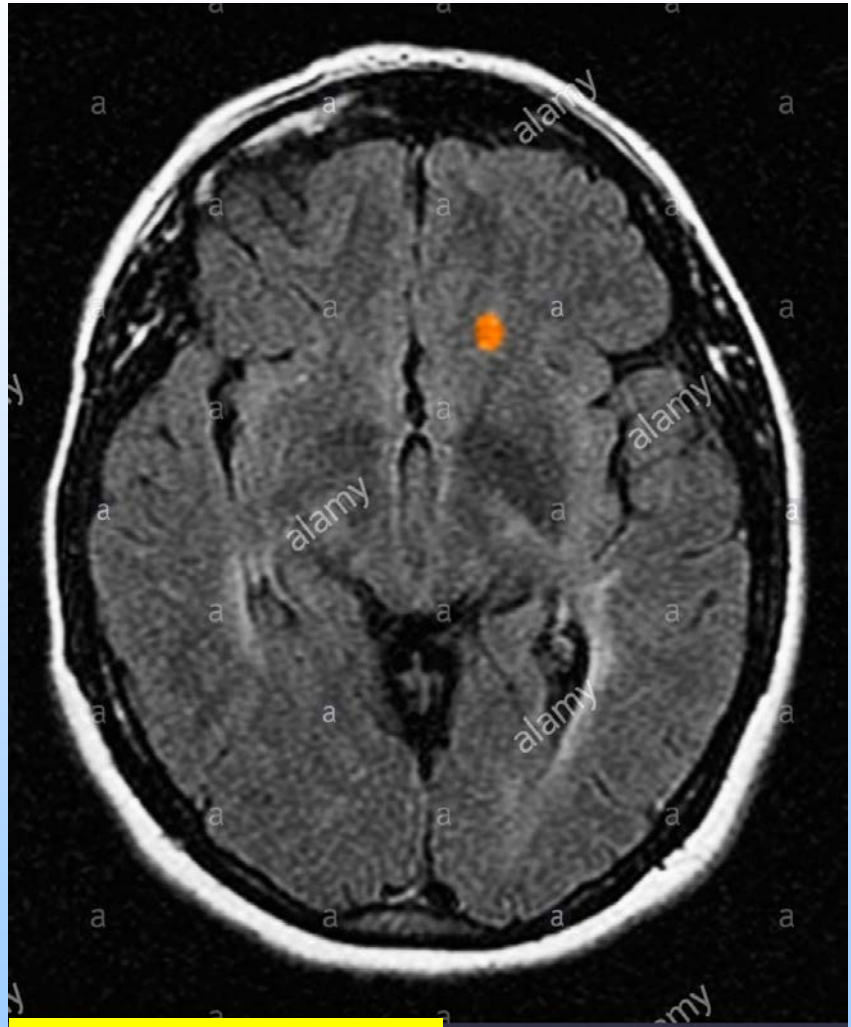

CT scan of a brain

Basics of acoustic tomography of the atmosphere (ATA)

The idea of ATA is similar to that of a CT scanner: using sound waves propagating through the atmosphere, we would like to reconstruct the temperature and wind velocity fields.

Shown is a horizontal slice (80 m x 80 m) of the wind velocity magnitude obtained with Large Eddy Simulations (LES). Arrows indicate the direction of the velocity and colors indicate the magnitude of the velocity. The spatial resolution is 4 m x 4 m with interpolation between grid cells. LES produces realistic temperature and wind velocity fields. The LES solves the Navier-Stocks equations which govern the temporal and spatial evolution of the temperature and wind velocity in the atmospheric boundary layer (ABL). The direct numerical simulation (DNS) of these equations is still computationally prohibitive. In the LES, small scale turbulence is not resolved and its effect on large scales is parameterized.

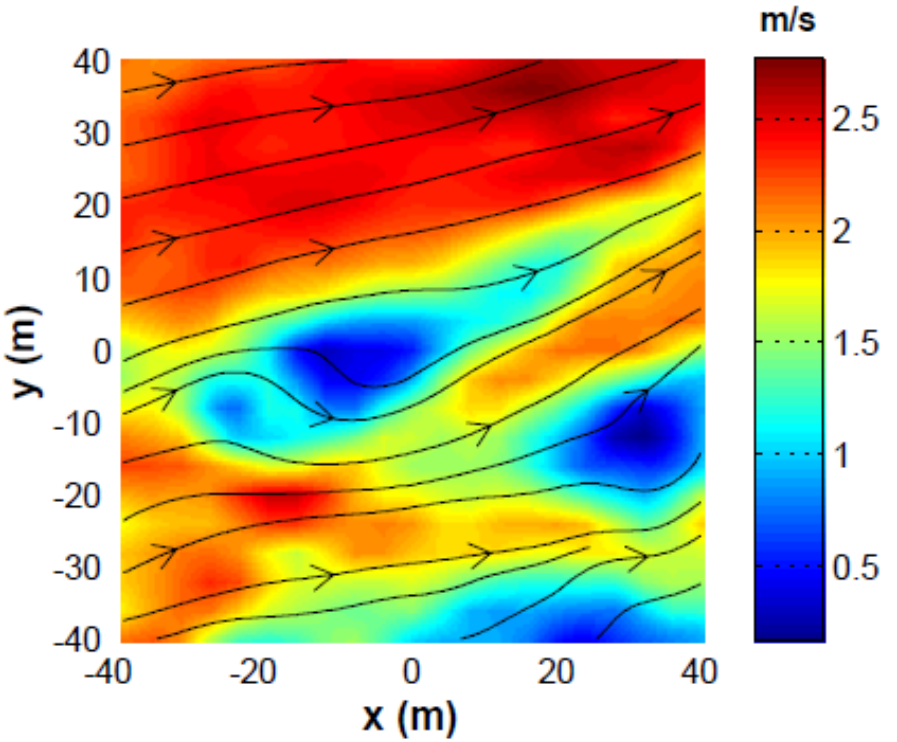

The goal of acoustic tomography of the atmosphere is to obtain experimentally such temperature and velocity fields.

Basics of ATA

A CT scanner is based on attenuation of x rays in a medium. ATA employs the fact that a travel time of sound waves in the atmosphere from a sound source (e.g., a speaker) to a microphone depends on the temperature and wind velocity along the propagation path. Therefore, ATA is also termed as travel-time acoustic tomography. (In principle, other parameters of sound signals such as attenuation can be measured with the goal of reconstructing other properties of the atmosphere, e.g., humidity fluctuations.)

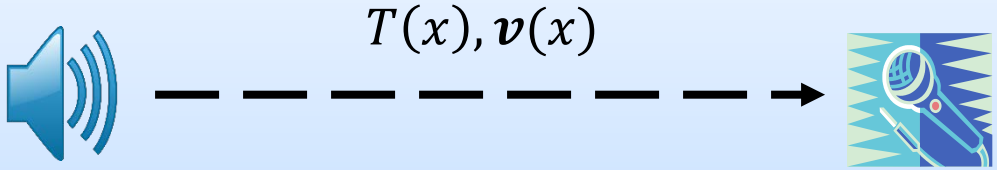

1. Forward problem in ATA: Express the travel time of sound signals in terms of the temperature and wind velocity fields and the coordinates of speakers and microphones.

2. Inverse problem in ATA: Reconstruct the temperature and wind velocity fields from the measured travel times.

Similarly to a CT scanner, in ATA we need many sound propagation paths and, hence, many speakers and microphones. A set of speakers and microphones with pertinent instrumentation is called an acoustic tomography array. As an example of a tomography array, we consider the array for acoustic tomography of the atmosphere built at the Boulder Atmospheric Observatory (BAO), located near Boulder, CO, USA.

2. BAO acoustic tomography array

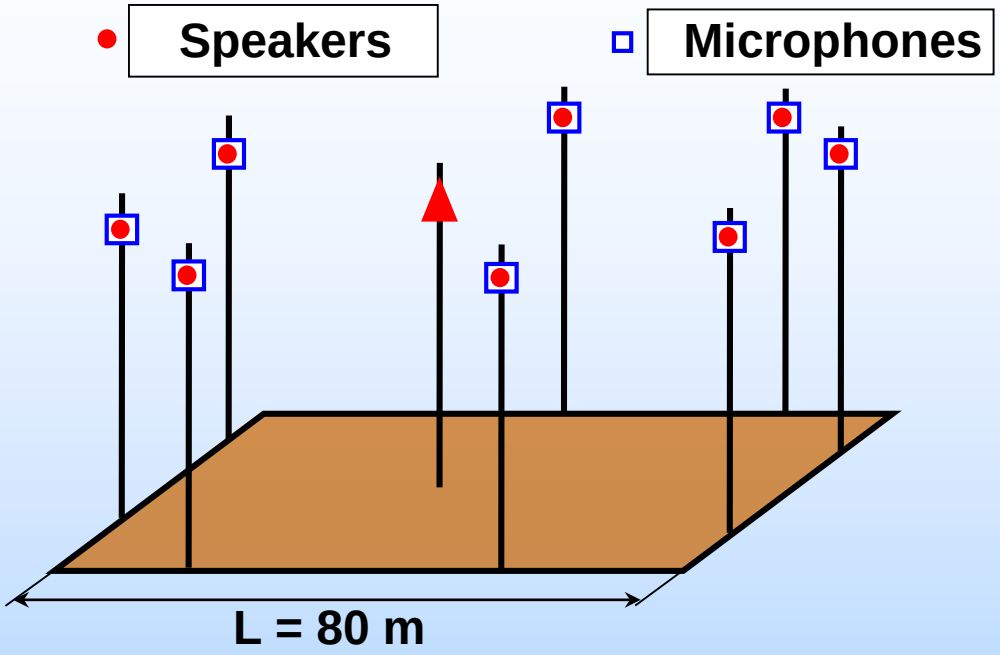

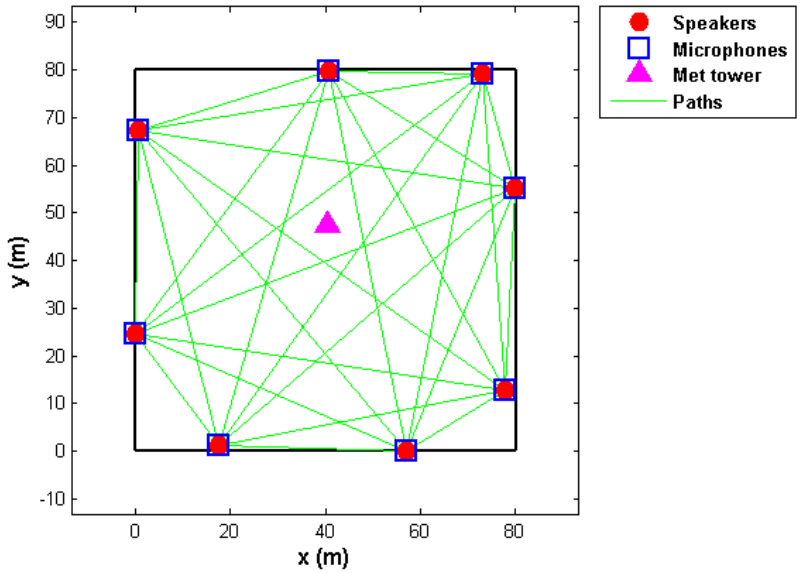

The BAO 2.0 acoustic tomography array consisted of 8 towers located along the perimeter of a square with the size 80 m x 80 m. Each tower carried a speaker and microphone at the height of about 8 m above the ground. The tower #9 in the middle of the array carried a sonic anemometer and a temperature probe. Right plot shows a view from above on the array; speakers and mics are located along the perimeter of a square. Green lines indicate 56 propagation paths. Principle of operation of the BAO 2.0 tomography array: eight speakers were activated in a sequence and transmitted short pulses. Microphones recorded these pulses. One cycle of transmission and recording lasted 0.5 s. This enabled us to determine the travel times of sound propagation along 56 paths every 0.5 s. Then, this cycle was repeated for up to a few hours. (The tomography array was dismantled in 2016 due to decommission of the BAO.) The BAO 1.0 tomography array had the same 8 towers, but 3 towers carried only speakers and the remaining 5 towers carried only mics resulting in 15 paths.

Block diagram of the BAO tomography array

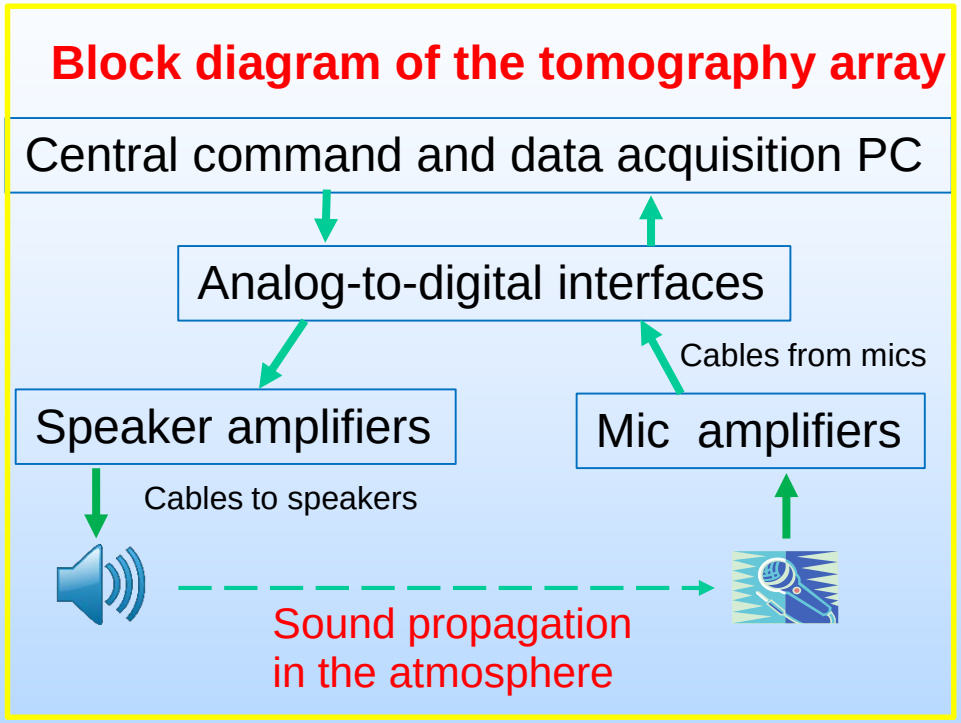

Shown is the block diagram of the BAO tomography array. A LabVIEW program was written to run the tomography array from the central command and data acquisition PC and store all data on the PC. Speakers were activated by this program via A/D interfaces, speaker amplifiers, and cables to the towers. Then, sound pulses propagated in the atmosphere and were recorded by microphones. The microphone signals were amplified and recorded by the PC via A/D interfaces. Simultaneously, the PC recorded the wind velocity and temperature (via a sonic anemometer and temperature probe).

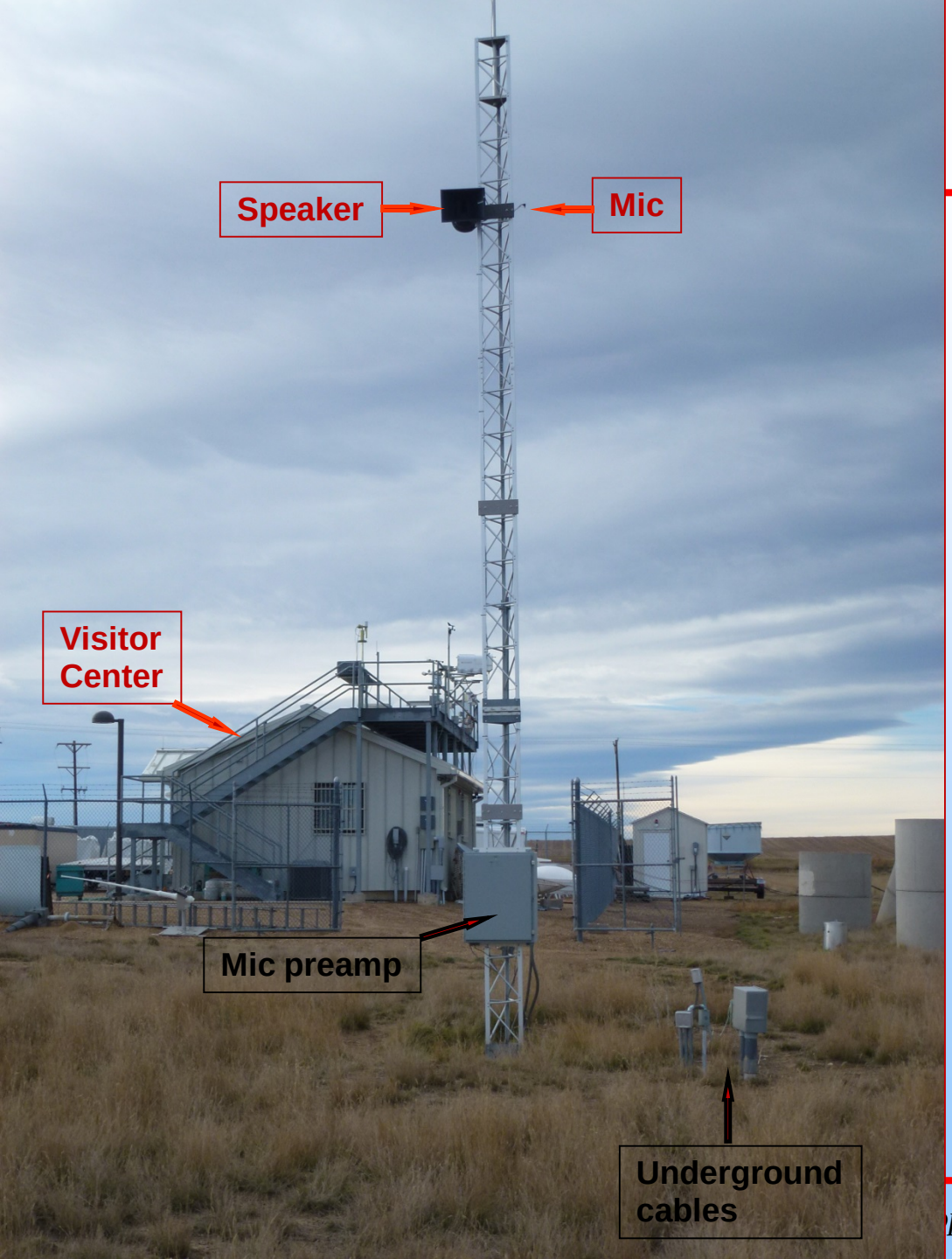

One of the towers of the BAO array

Shown is tower #5 of the BAO tomography array. The tower is 9.1 m high. A speaker and a mic were installed at 8 m above the ground. The instrumentation box carried a mic preamp and power outlet. A building behind the tower is the BAO Visitor Center (VC), where the acoustic tomography operation center was located. Cables in underground conduits connected the towers with the acoustic tomography operation center.

Eight towers of the BAO tomography array and the VC

Acoustic tomography operation center

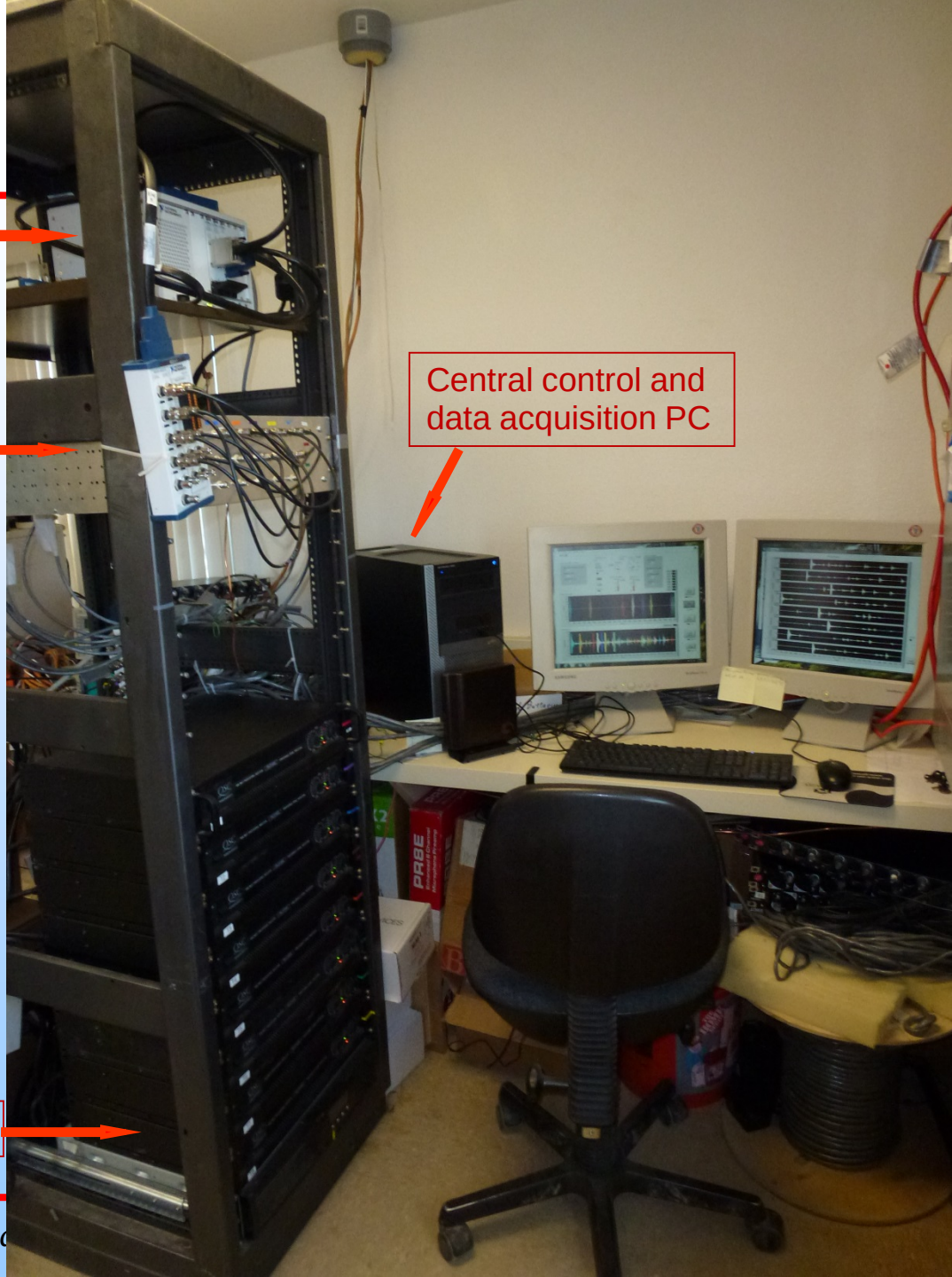

The acoustic tomography operation center inside the Visitor Center. The central command and data acquisition PC is on the desk. Two monitors show 8 transmitted signal and 8 signals recorded by microphones. The rack carries the A/D interfaces, power amplifiers for speakers, and mic filters. Cables to the towers can be seen on the right.

Transmitted signal

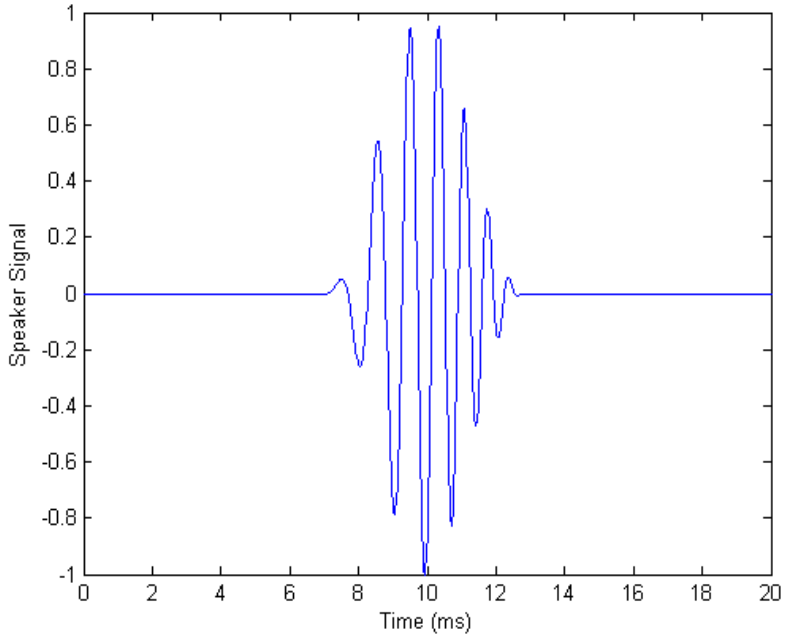

Received signal

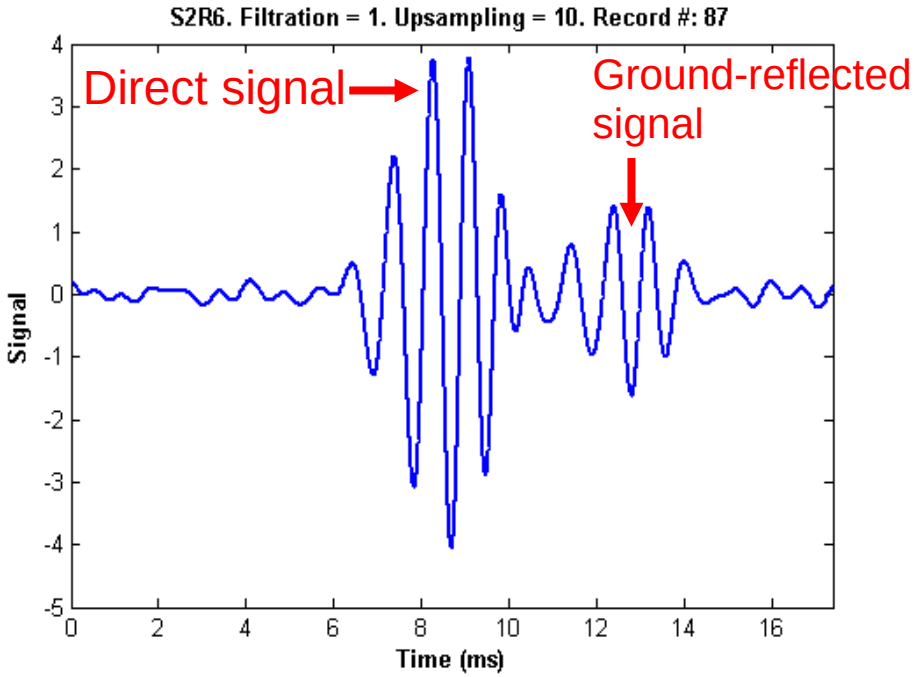

Shown are the transmitted and received signals. Transmitted signal: a chirp with the central frequency 1.2 kHz and duration of 5.8 ms. The received signal consists of the direct signal and that reflected from the ground. Cross-correlation of the transmitted and received signals enables determination of the travel time of sound propagation between a speaker and microphone. The ground reflected signal might be used to reconstruct 3D temperature and velocity fields.

Temporal evolution of the travel time

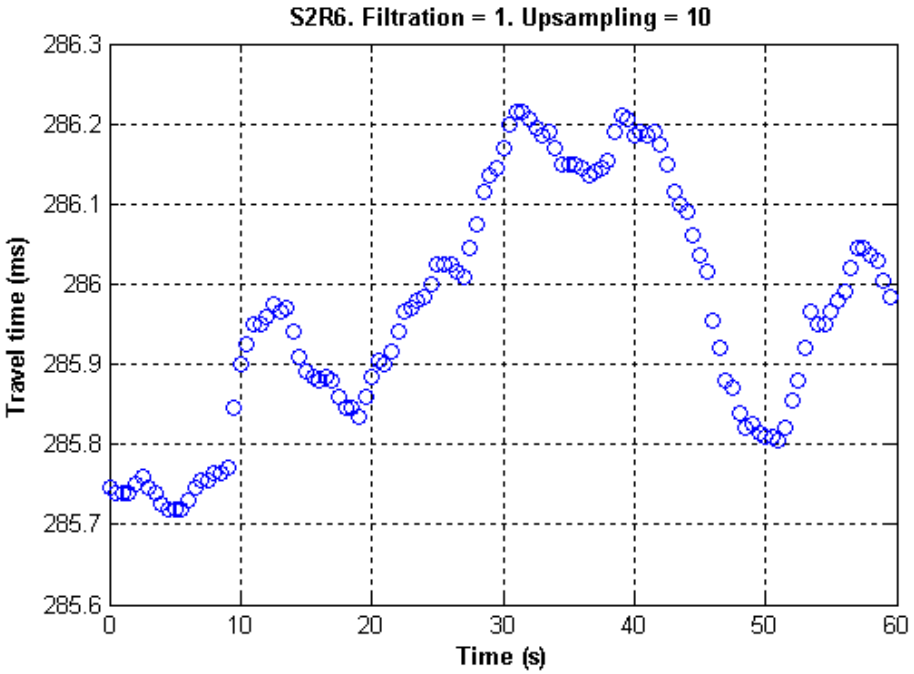

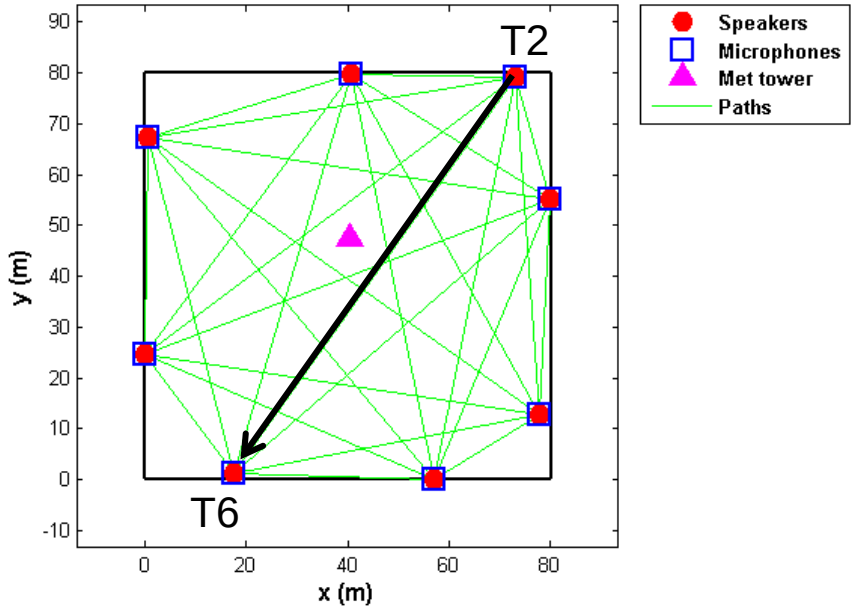

The travel time of sound propagation from speaker T2 to mic T6 during 1 min (120 transmissions). The travel time gradually changes from one measurement to another due to changing temperature and velocity fields along the path. A maximum deviation of the travel time is about 0.5 ms. The travel times for other propagation paths were obtained.

Next step in ATA is reconstruction of the temperature and velocity fields from the travel times.

3. Forward and inverse problems in ATA

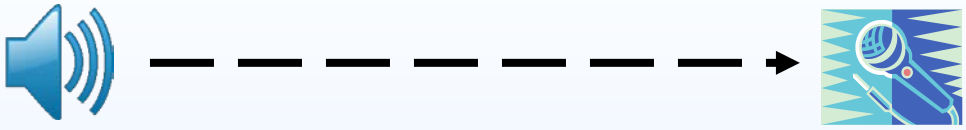

The forward problem in ATA expresses the travel time τ of sound propagation from a speaker to a microphone in terms of the temperature T and wind velocity $\boldsymbol{v}$ along the path:

$$\tau = \int_{l_s}^{l_m} \frac{dl}{u_{\mathrm{gr}}(l)}, \qquad \boldsymbol{u}_{\mathrm{gr}} = c\boldsymbol{n} + \boldsymbol{v}, \qquad c = \sqrt{\gamma R_a T}.$$

Here, the integration is performed along a curved path from a speaker (l_s) to a microphone (l_m), u_{gr} is the magnitude of the group velocity of the sound wave, c is the sound speed, and $\boldsymbol{n}$ is the unit vector normal to the wave front. The sound speed and temperature are related by the well-known equation. The forward problem is formulated rigorously using geometrical acoustics in a moving medium:

Ostashev and Wilson, *Acoustics in Moving Inhomogeneous Media, 2nd Ed.* (CRC Press, 2015).

The temperature, sound speed, and wind velocity are expressed as mean values (averaged over the tomographic area) and fluctuations. The forward problem is linearized assuming that the propagation path is relatively small and that $\tilde{T} \ll T$ and $\tilde{v} \ll c_0$.

$$T(\boldsymbol{r}) = T_0 + \tilde{T}(\boldsymbol{r}), \;\; \mathrm{c}(\boldsymbol{r}) = c_0 + \tilde{c}(\boldsymbol{r}), \;\; \boldsymbol{v}(\boldsymbol{r}) = \boldsymbol{v}_0 + \tilde{\boldsymbol{v}}(\boldsymbol{r}). \;\; \boldsymbol{r} = (x, y).$$

Linearized forward problem in ATA

Linearized forward problem for the travel time of sound propagation along the i propagation path:

$$\tau_i = \frac{L_i}{c_0}\left(1 - \frac{\boldsymbol{s}_i \cdot \boldsymbol{v}_0}{c_0}\right) - \frac{1}{c_0}\int_{L_i}\left[\frac{\tilde{T}(\boldsymbol{r})}{2T_0} + \frac{\boldsymbol{s}_i \cdot \tilde{\boldsymbol{v}}(\boldsymbol{r})}{c_0}\right] dl, \qquad i = 1, 2, \ldots, I.$$

Here, the first term is due to the mean temperature and velocity and the second term is due to their fluctuations. Integration is done along the straight line from a speaker to a mic, $\boldsymbol{s}_i$ is the unit vector in the direction of this line, and L_i is the path length. For the BAO tomography array $I = 56$. The mean sound speed and velocity can be measured with a sonic and T-probe or reconstructed using a least square estimation as explained below. This enables us to determine the vector

$$d_i = c_0 L_i\left(1 - \frac{\boldsymbol{s}_i \cdot \boldsymbol{v}_0}{c_0}\right) - c_0^2 \tau_i,$$

which we call the data for reconstruction of the fluctuations. From these equations, we obtain the linearized forward problem for temperature and velocity fluctuations

$$d_i = c_0 \int_{L_i}\left[\frac{\tilde{T}(\boldsymbol{r})}{2T_0} + \frac{\boldsymbol{s}_i \cdot \tilde{\boldsymbol{v}}(\boldsymbol{r})}{c_0}\right] dl.$$

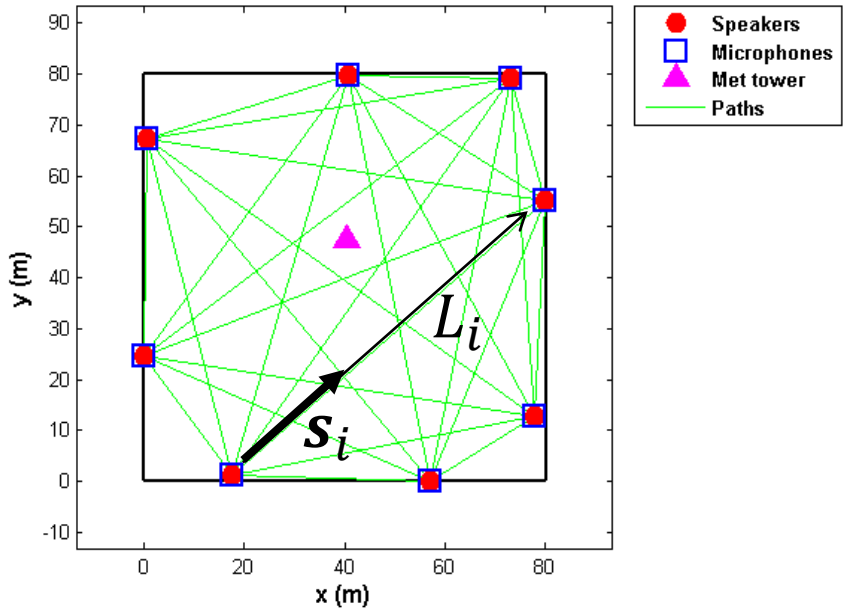

Inverse problem in ATA

The linearized forward problem for T and v fluctuations

$$d_i = c_0 \int_{L_i} \left[\frac{\tilde{T}(\boldsymbol{r})}{2T_0} + \frac{\boldsymbol{s}_i \cdot \tilde{\boldsymbol{v}}(\boldsymbol{r})}{c_0} \right] dl + \varepsilon_i,$$

where ε_i is noise in the data. The column vector of data

$$\boldsymbol{d} = [d_1; d_2; \ldots d_I], \qquad i = 1, 2, \ldots, I.$$

The tomographic area is divided into J grid cells, in which $\tilde{T}(\boldsymbol{r})$ and $\tilde{\boldsymbol{v}}(\boldsymbol{r})$ are assumed constant and termed models. The column vector of models has *3J* components:

$$\mathbf{m} = \left[\tilde{T}_1; \tilde{T}_2; \ldots \tilde{T}_J; \tilde{v}_{x1}; \tilde{v}_{x2}; \ldots \tilde{v}_{xJ}; \tilde{v}_{y1}; \tilde{v}_{y2}; \ldots \tilde{v}_{yJ}\right].$$

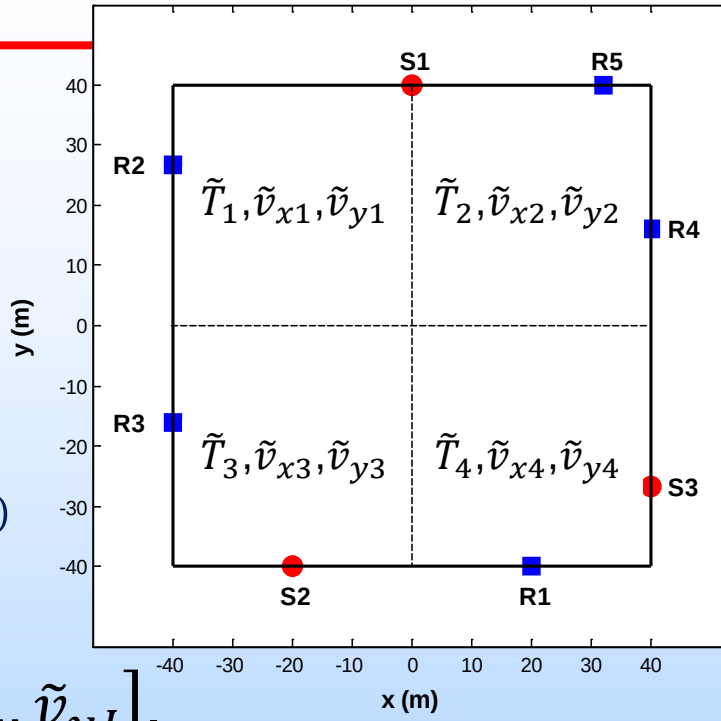

An inverse problem in ATA is to solve the forward problem for $\boldsymbol{m}$. The solution is termed as an estimation (reconstruction) of models and differs from the models:

$$\hat{\mathbf{m}} = \left[\hat{T}_1; \hat{T}_2; \ldots \hat{T}_J; \hat{v}_{x1}; \hat{v}_{x2}; \ldots \hat{v}_{xJ}; \hat{v}_{y1}; \hat{v}_{y2}; \ldots \hat{v}_{yJ}\right].$$

There are many approaches for the inverse problem, e.g., an algebraic reconstruction. For T and v constant in grid cells, the integrals in the forward problem are calculated analytically.

Algebraic reconstruction

The forward problem in the algebraic reconstruction becomes:

$$d_i = \sum_{j=1}^{J} \left(a_{ij} \tilde{T}_j + b_{ij}^x \tilde{v}_{xj} + b_{ij}^y \tilde{v}_{yj} \right) + \varepsilon_i,$$

The data for path i are expressed in terms of the models (temperature and two velocity components in the grid cells) and the matrices a_{ij}, b_{ij}^x, and b_{ij}^y which depend on the transducer's coordinates. The forward problem can be written in a matrix form:

$$\boldsymbol{d} = \boldsymbol{M}\boldsymbol{m} + \boldsymbol{\varepsilon}, \qquad \text{where} \qquad \boldsymbol{M} = \left[a_{ij}, b_{ij}^x, b_{ij}^y \right], \quad \boldsymbol{\varepsilon} = [\varepsilon_1; \varepsilon_2, \ldots \varepsilon_I].$$

In the inverse problem, we solve this equation for $\boldsymbol{m}$. The damped least square (DLS) estimation yields:

$$\hat{\mathbf{m}} = (\boldsymbol{M}^T \boldsymbol{M} + \alpha \boldsymbol{I})^{-1} \boldsymbol{M}^T \boldsymbol{d},$$

which expresses $\hat{\mathbf{m}}$ in terms of the column vector of the data $\boldsymbol{d}$. Here, the subscript T indicates the transpose of a matrix, "-1" means the inverse of a matrix, α is the regularization parameter, and $\boldsymbol{I}$ is the identity matrix. The DLS estimation minimizes the difference

$$(\boldsymbol{M}\hat{\mathbf{m}} - \boldsymbol{M}\boldsymbol{m})^2 \longmapsto \min.$$

Algebraic reconstruction

$$\hat{\mathbf{m}} = (\boldsymbol{M}^T\boldsymbol{M} + \alpha\boldsymbol{I})^{-1}\,\boldsymbol{M}^T\boldsymbol{d}.$$

The DLS estimation works very well if the number of the data (the length of $\boldsymbol{d}$) is greater than the number of models (the length of $\boldsymbol{m}$): $I > 3J$, i.e., the inverse problem is overdetermined. This is the case for a CT scanner.

In ATA, we would like to reconstruct the T and v fields similar to those obtained with LES, where the spatial resolution is 4 m x 4 m. In this case the number of grid cells is *J = 400* and the number of models is *3J = 1200*! Even for a not very good spatial resolution 16 m x 16 m (right plot), the number of models *3 x J = 3 x 25 = 75* exceeds the number of data *I = 56.* Thus, the inverse problem in ATA is intrinsically underdetermined.

The algebraic reconstruction cannot be used in ATA and we need a good algorithm for solution of undetermined inverse problems.

LES

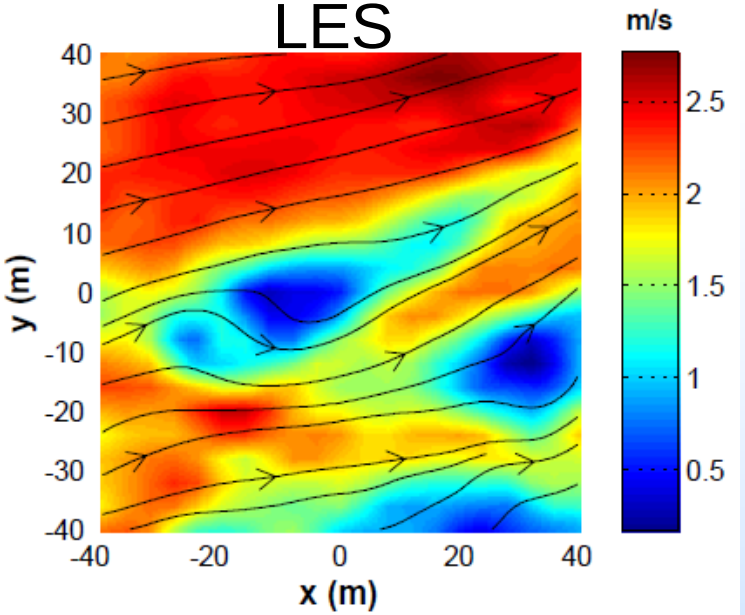

BAO 1.0 tomography array

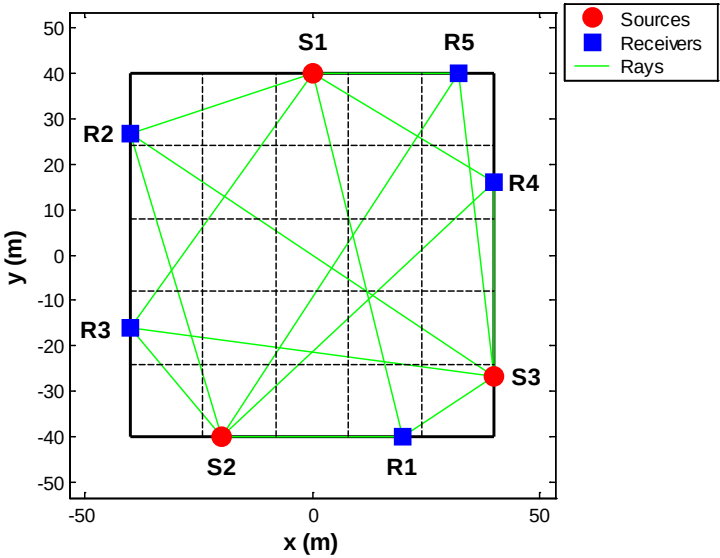

Stochastic inversion (SI)

Another shortcoming of the algebraic reconstruction is that the models within two grid cells are assumed uncorrelated. However, if we measure the temperature fluctuations at two spatial points, $\boldsymbol{r}_1$ and $\boldsymbol{r}_2$, multiply the result, and average over time, we obtain the spatial correlation function of temperature fluctuations:

$$B_T(\boldsymbol{r}_1 - \boldsymbol{r}_2) = \frac{1}{\Delta t}\int_{t_0}^{t_0+\Delta t} \tilde{T}(\boldsymbol{r}_1, t)\tilde{T}(\boldsymbol{r}_2, t)dt.$$

This correlation function is not zero if the two points are located relatively close to each other.

A stochastic inversion employs the fact that the temperature and wind velocity fluctuations are spatially correlated and is used to solve underdetermined inverse problems.

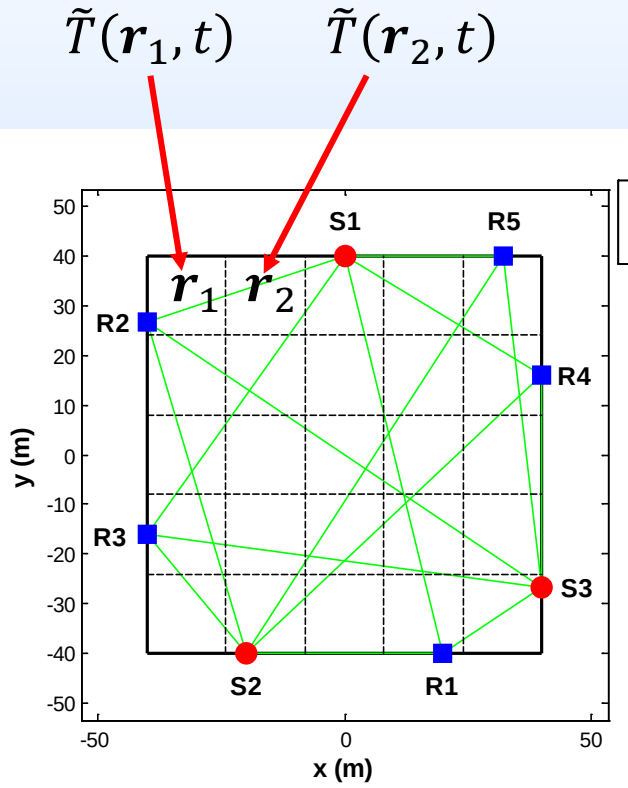

Stochastic inversion

The linearized forward problem for T and v fluctuations is given by the same equations:

$$d_i = c_0 \int_{L_i} \left[\frac{\tilde{T}(\boldsymbol{r})}{2T_0} + \frac{\boldsymbol{s}_i \cdot \tilde{\boldsymbol{v}}(\boldsymbol{r})}{c_0} \right] dl + \varepsilon_i, \quad \boldsymbol{d} = [d_1; d_2; \dots d_I],$$

However, $\tilde{T}(\boldsymbol{r})$ and $\tilde{\boldsymbol{v}}(\boldsymbol{r})$ are now random functions with known spatial correlation functions. The tomographic area is again divided into J grid cells, in which $\tilde{T}(\boldsymbol{r})$ and $\tilde{\boldsymbol{v}}(\boldsymbol{r})$ are constant random values

$$\mathbf{m} = \left[\tilde{T}(\boldsymbol{r}_1); \tilde{T}(\boldsymbol{r}_2); \dots \tilde{T}(\boldsymbol{r}_J); \tilde{v}_x(\boldsymbol{r}_1); \tilde{v}_x(\boldsymbol{r}_2); \dots \tilde{v}_x(\boldsymbol{r}_J); \tilde{v}_y(\boldsymbol{r}_1); \tilde{v}_y(\boldsymbol{r}_2); \dots \tilde{v}_y(\boldsymbol{r}_J)\right].$$

The estimation of the models are not random:

$$\hat{\mathbf{m}} = \left[\hat{T}(\boldsymbol{r}_1); \hat{T}(\boldsymbol{r}_2); \dots \hat{T}(\boldsymbol{r}_J); \hat{v}_x(\boldsymbol{r}_1); \hat{v}_x(\boldsymbol{r}_2); \dots \hat{v}_x(\boldsymbol{r}_J); \hat{v}_y(\boldsymbol{r}_1); \hat{v}_y(\boldsymbol{r}_2); \dots \hat{v}_y(\boldsymbol{r}_J)\right].$$

The stochastic inversion minimizes the deviation of the estimations from the models, where the brackets $\langle \quad \rangle$ indicate averaging over an ensemble of realizations of T and v fluctuations:

$$\left\langle \left(\hat{m}_j - m_j\right)^2 \right\rangle \longmapsto \min, \qquad j = 1, 2, \dots J.$$

Stochastic inversion

Similarly to the algebraic reconstruction, the estimation of the models is expressed in terms of the column vector of the data, but with a different matrix on the right-hand side:

$$\hat{\mathbf{m}} = \boldsymbol{R}_{md}\boldsymbol{R}_{dd}^{-1}\boldsymbol{d}.$$

$$\boldsymbol{R}_{md} = \langle \boldsymbol{m}\boldsymbol{d}^T \rangle = \frac{c_0}{2T_0}\int_{L_i} B_T\big(\boldsymbol{r}_j - \boldsymbol{r}(l_i)\big)dl_i\,,\ j = 1,2,\ldots J,\quad i = 1,2,\ldots I.$$

$$\boldsymbol{R}_{dd} = \langle \boldsymbol{d}\boldsymbol{d}^T \rangle = \frac{c_0^2}{4T_0^2}\int_{L_i} dl_i \int_{L_k} B_T(\boldsymbol{r}(l_i) - \boldsymbol{r}(l_k))\, dl_k\,,\ k = 1,2,\ldots I.$$

Here, $\boldsymbol{R}_{md}$ and $\boldsymbol{R}_{dd}$ are the model-data and data-data covariance matrices which are expressed in terms of $B_T(\boldsymbol{r})$. In $\boldsymbol{R}_{md}$, the integration is done along the *i* path. In $\boldsymbol{R}_{dd}$, the integration is done along the paths *i* and *k*. The velocity fluctuations are accounted similarly. The SI also provides the estimated errors of reconstruction in each grid cell, where $\boldsymbol{R}_{mm} = \langle \boldsymbol{m}\boldsymbol{m}^T \rangle$ is the model-model covariance matrix:

$$\boldsymbol{R}_{ee} = \boldsymbol{R}_{mm} - \boldsymbol{R}_{md}\boldsymbol{R}_{dd}^{-1}\boldsymbol{R}_{md}^T.$$

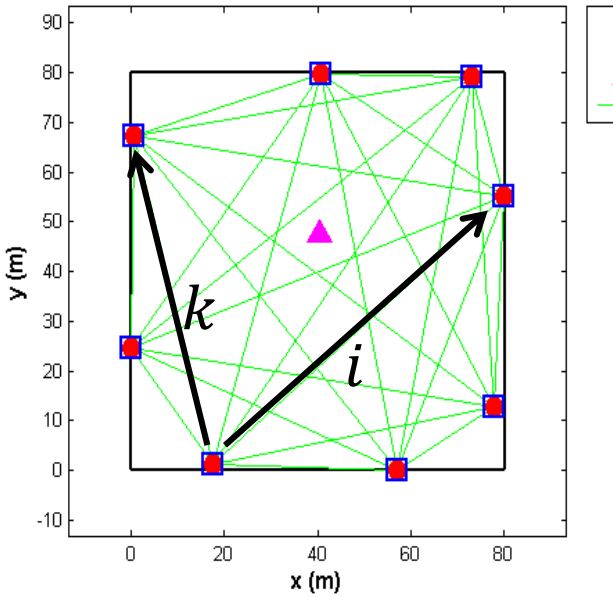

Time-dependent stochastic inversion (TDSI)

The SI had been known in the literature and when applied to ATA, this was a step forward. Vecherin et al. (2006) developed even a better algorithm for the T and v reconstruction, which is termed the time-dependent stochastic inversion (TDSI). In TDSI, we take into account that T and v fluctuations correlate not only in space, but also in time. For frozen turbulence, the T and v fluctuations (such as those in the right plot) move with the mean wind, thus resulting in the spatial-temporal correlations. By repeated measurements of the travel times τ_i at close time moments t_1, t_2, … t_N and accounting for these correlations, we obtain more data for the tomographic reconstruction.

In the BAO tomography array, the travel times were measured every 0.5 s (right plot). In TDSI, N sets of the travel times τ_i are used for the reconstruction of T and v fluctuations:

$$\tau_i(t_1), \tau_i(t_2), \ldots \tau_i(t_N).$$

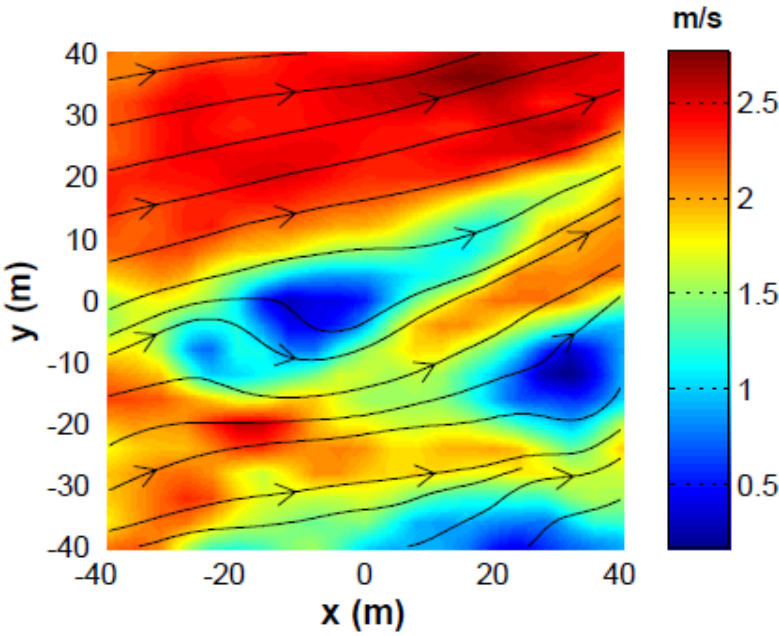

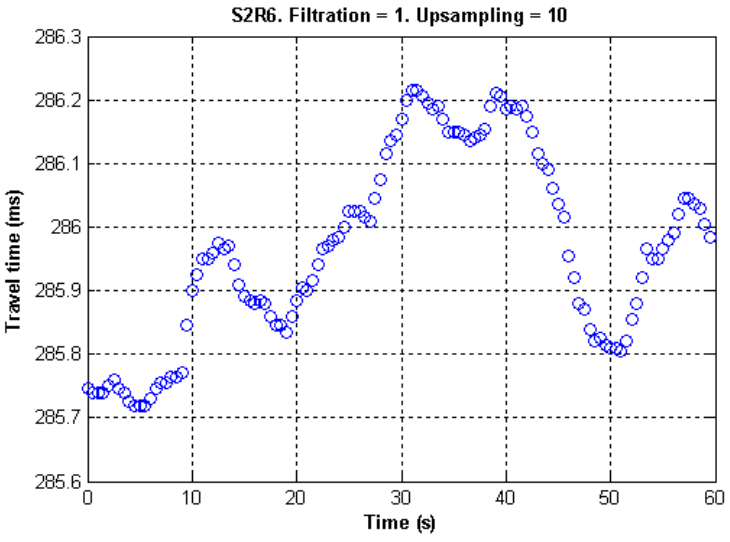

Time-dependent stochastic inversion

This enables to obtain N sets of the data at the time moments t_1, t_2, … t_N :

$$\boldsymbol{d} = [\boldsymbol{d}(t_1); \boldsymbol{d}(t_2); \ldots \boldsymbol{d}(t_N)].$$

The models are also specified at the time moments t_1, t_2, … t_N:

$$\boldsymbol{m} = [\boldsymbol{m}(t_1); \boldsymbol{m}(t_2); \ldots \boldsymbol{m}(t_N)].$$

The estimation of the models is done at one time moment t_0, for which: $t_1 < t_0 < t_N$,

$$\hat{\mathbf{m}}(t_0) = \left[\hat{T}(\boldsymbol{r}_1, t_0); \ldots \hat{T}(\boldsymbol{r}_J, t_0); \hat{v}_x(\boldsymbol{r}_1, t_0); \ldots \hat{v}_x(\boldsymbol{r}_J, t_0); \hat{v}_y(\boldsymbol{r}_1, t_0); \ldots \hat{v}_y(\boldsymbol{r}_J, t_0)\right].$$

The solution of the inverse problem is given by the same formula as for the SI. However, the column vector of the data has now many more components.

$$\hat{\mathbf{m}} = \boldsymbol{R}_{md}\boldsymbol{R}_{dd}^{-1}\boldsymbol{d}; \qquad \boldsymbol{R}_{md} = \langle \boldsymbol{m}\boldsymbol{d}^T \rangle, \quad \boldsymbol{R}_{dd} = \langle \boldsymbol{d}\boldsymbol{d}^T \rangle.$$

Thus, by repeated measurements of the travel times and accounting for the spatial-temporal correlations in the T and v fields, TDSI allows us to increase the amount of data without increasing the number of speakers and microphones. Development of this algorithm was a breakthrough in ATA. TDSI generalizes SI and is similar to the Kalman filter (e.g., Kolouri et al., 2014). In principle, SI and TDSI enable the tomographic reconstruction on a very small grid; there is, however, a tradeoff between the spatial resolution and the errors in reconstruction.

4. Numerical simulations of the BAO tomography array

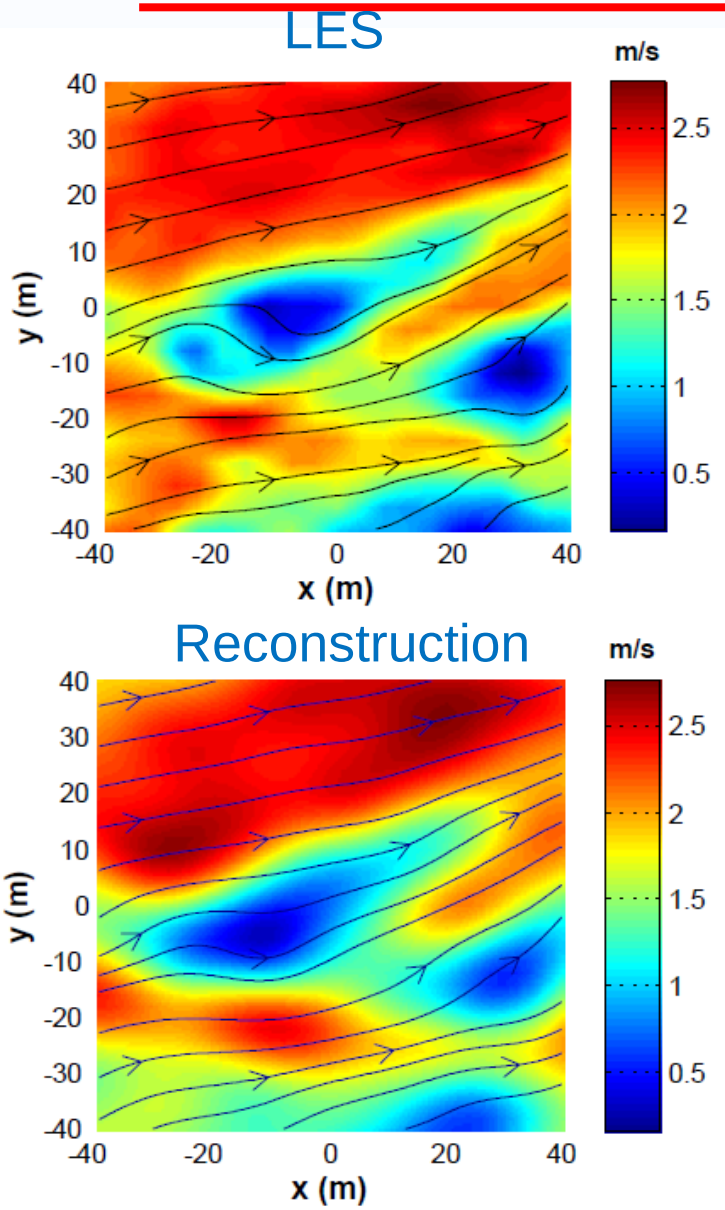

TDSI was used in numerical simulations of the BAO tomography array. The upper plot is the wind velocity magnitude obtained with LES. Arrows indicate the direction of the velocity. This LES field was moving through the tomography array; the travel times of sound pulses were calculated every 0.5 s and corrupted by noise. Five consecutive sets of the travel times were used and the spatial resolution was 4 m x 4 m with interpolation between the grid cells. The lower plot is the tomographic reconstruction of the velocity. The reconstruction reproduces correctly the main features of the LES field: the arrows are pointed in the same direction and fast and slow eddies are reproduced accurately. The results are available as movies.

The accuracy of a tomographic reconstruction of the temperature and velocity depends on many factors such as the number of transducers, the errors in measurements of the travel times and transducers coordinates, location of transducers, and inverse algorithms. In TDSI, it can be as good as 0.1 C for T and 0.1 m/s for **v**. The temporal resolution can be about 0.25 s. An algorithm was developed for finding an optimal location of speakers and microphones of the BAO array.

Calibration of the BAO tomography array

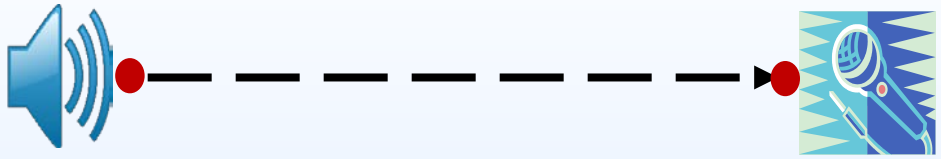

The BAO tomography array was accurately calibrated:

(i) The coordinates of the speakers and microphones were measured with a laser finder.

(ii) The time delays in the hardware and electronic system of the tomography array were determined for every pair of a speaker-microphone.

(iii) The forward problem in ATA is formulated for a point source and receiver. A mic can be considered as a point receiver. But a speaker consists of a driver and horn, and is not a point source. The effective point of emission is different in different azimuthal directions. This was accounted for by special measurements.

Tomography experiment at the BAO on 9 November 2014

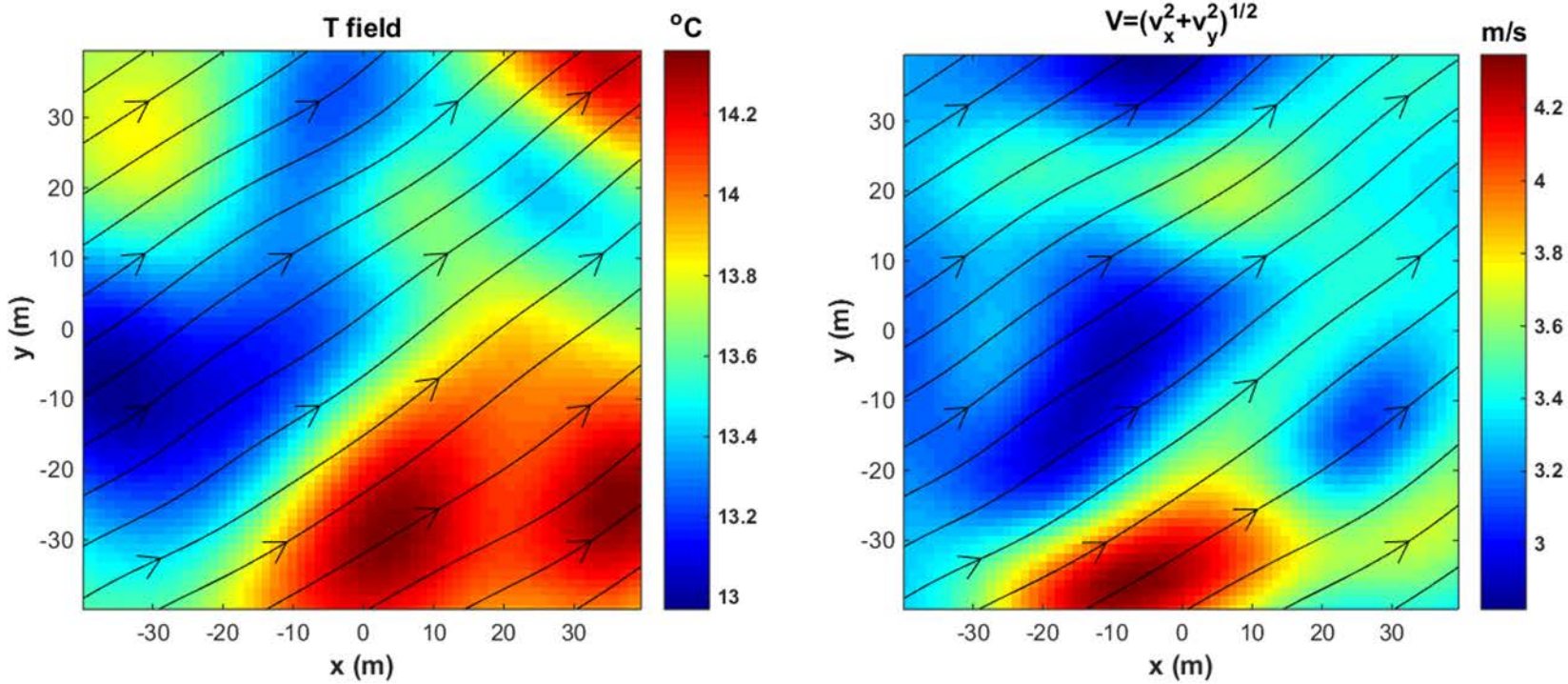

Shown are the temperature and wind velocity fields reconstructed with TDSI from the travel times measured with the BAO tomography array in November 2014. Five sets of the travel times were used and the spatial resolution was 4 m x 4 m. Arrows indicate the wind direction. Several “cold” and “warm” temperature eddies and “slow” and “fast” velocity eddies with different scales are seen in the plots. The eddies are reliably resolved since the expected errors in the reconstruction are less than the difference in temperature and velocity between the eddies. The temperature and velocity reconstructed in the center of the BAO array agree with those measured by a sonic anemometer and T-probe.

ATA for wind energy applications

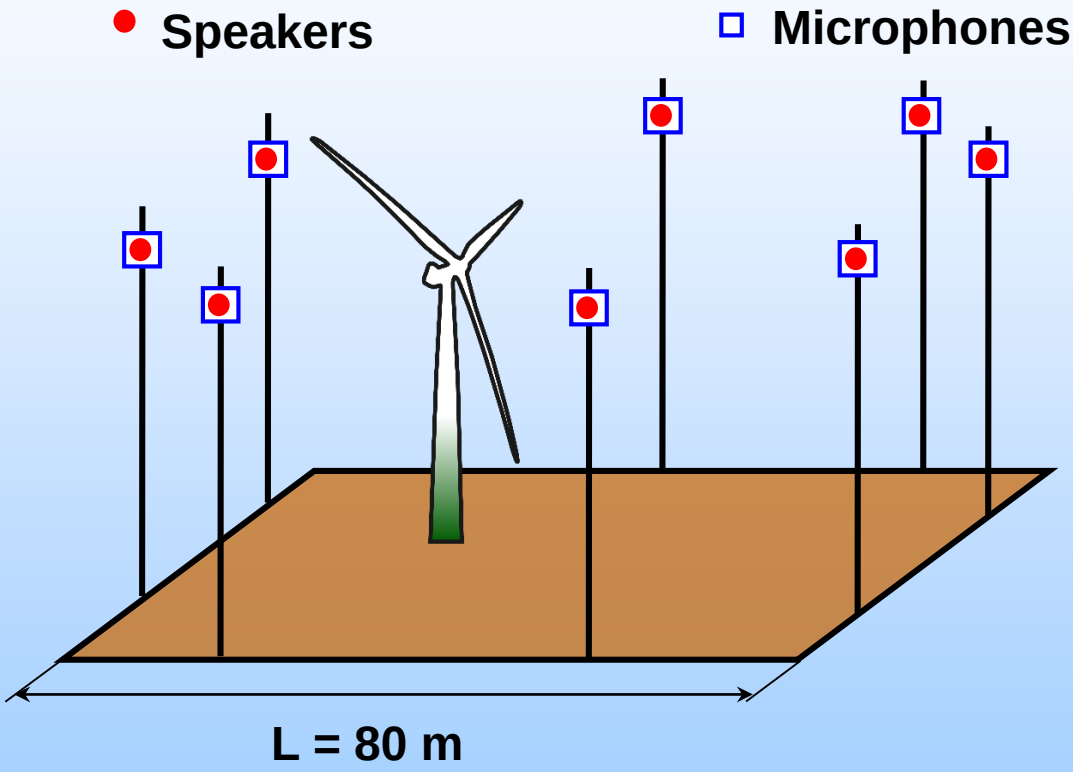

Our tomography array was dismantled in 2016 due to decommission of the BAO. It is now being rebuild at the National Wind Turbine Center (NWTC), located near Boulder, CO. The array will be used to monitor turbulent flows (including a wind turbine wake) near a small wind turbine. Experience gained in this project will allow us to scale acoustic tomography of an incoming turbulent flow and a wind turbine wake to large turbines. This is important for wind energy applications. There is currently no adequate instrumentation for such remote sensing.

Other applications of ATA

- Visualization of 4D dynamic processes in the atmosphere or in a wind tunnel.
- Experimental validation of high-resolution model simulations such as LES. ATA is particularly well suited for this purpose since it enables area-averaged measurements of the temperature and wind velocity fields to be compared with area-averaged results of LES.
- Studies of turbulence over complex topography.
- Input data for atmospheric models and wave propagation codes.

- Advantages of acoustic tomography in comparison with conventional meteorological devices: (i) These devices can perturb the temperature and velocity fields while acoustic tomography does not. (ii) Volume-imaging lidars cannot be used directly for remote sensing of temperature fluctuations. (iii) Acoustic tomography requires fewer sensors per unit of data than do conventional meteorological devices.

5. Other schematics and techniques for ATA

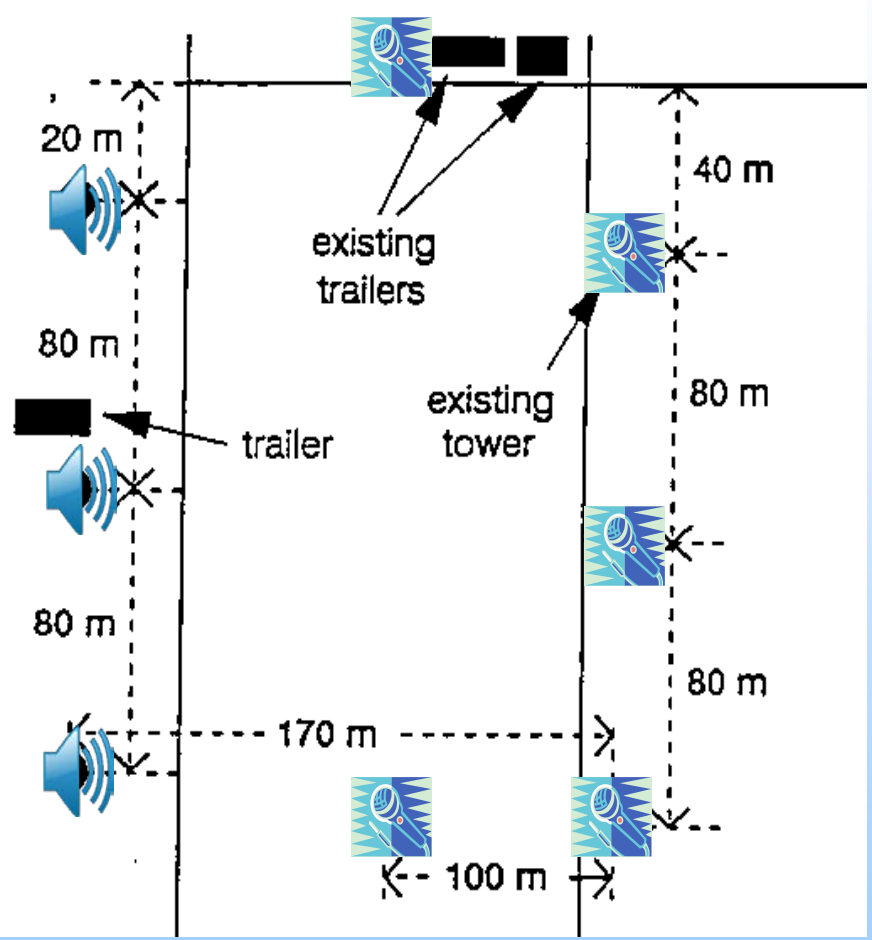

So far, we have considered ATA using the BAO tomography array as an example. In the remaining part of the presentation, we will overview similar tomography arrays and remote sensing techniques which can be termed as ATA.

Application of horizontal-slice tomography to near-ground atmosphere was first suggested by Spiesberger (1990).

First experimental implementation was reported by Wilson and Thomson (1994). Three speakers and five microphones were located 6 m above the ground along the perimeter of a square with the side length of 200 m, resulting in 15 propagation paths. SI was used to reconstruct the T and v fields.

Acoustic tomography array at the University of Leipzig, Germany.

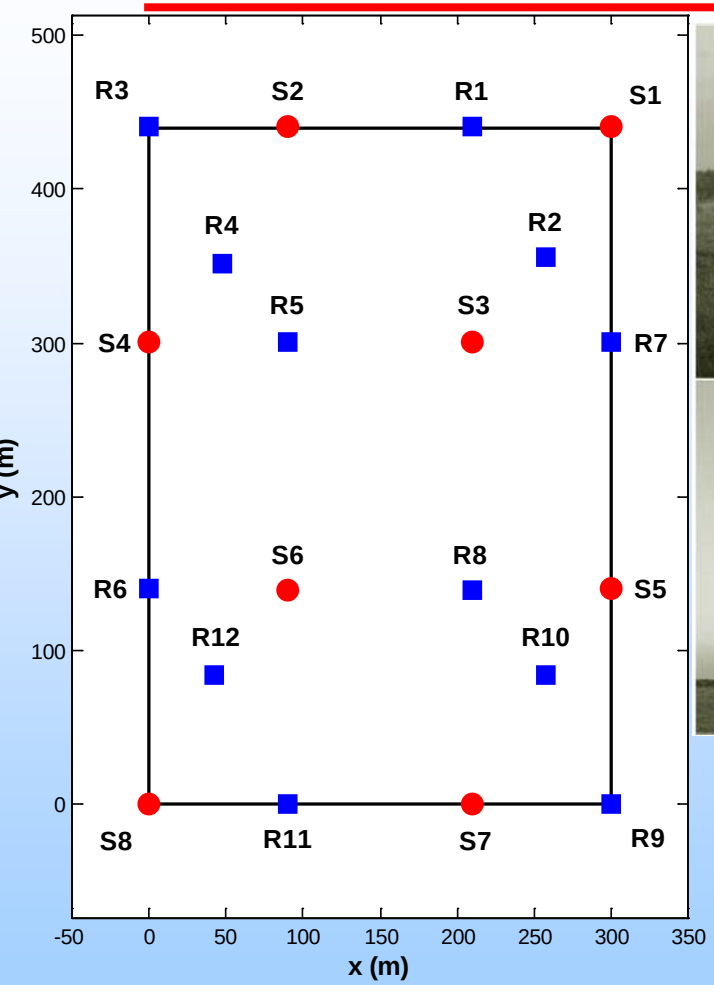

In the mid 1990's, scientists at the University of Leipzig built a portable acoustic tomography array and since then, have used it in many experimental campaigns. Speakers and mics were mounted on tripods 2 m above the ground. The size of the array varied and was of the order of several hundred meters. The German group used the algebraic reconstruction and, later, SI.

The left plot shows locations of 8 speakers and 12 microphones in the acoustic tomography experiment STINHO carried out in July 2002. The size the array was 300 m x 440 m. The travel times were measured every minute.

Site of the STINHO experiment

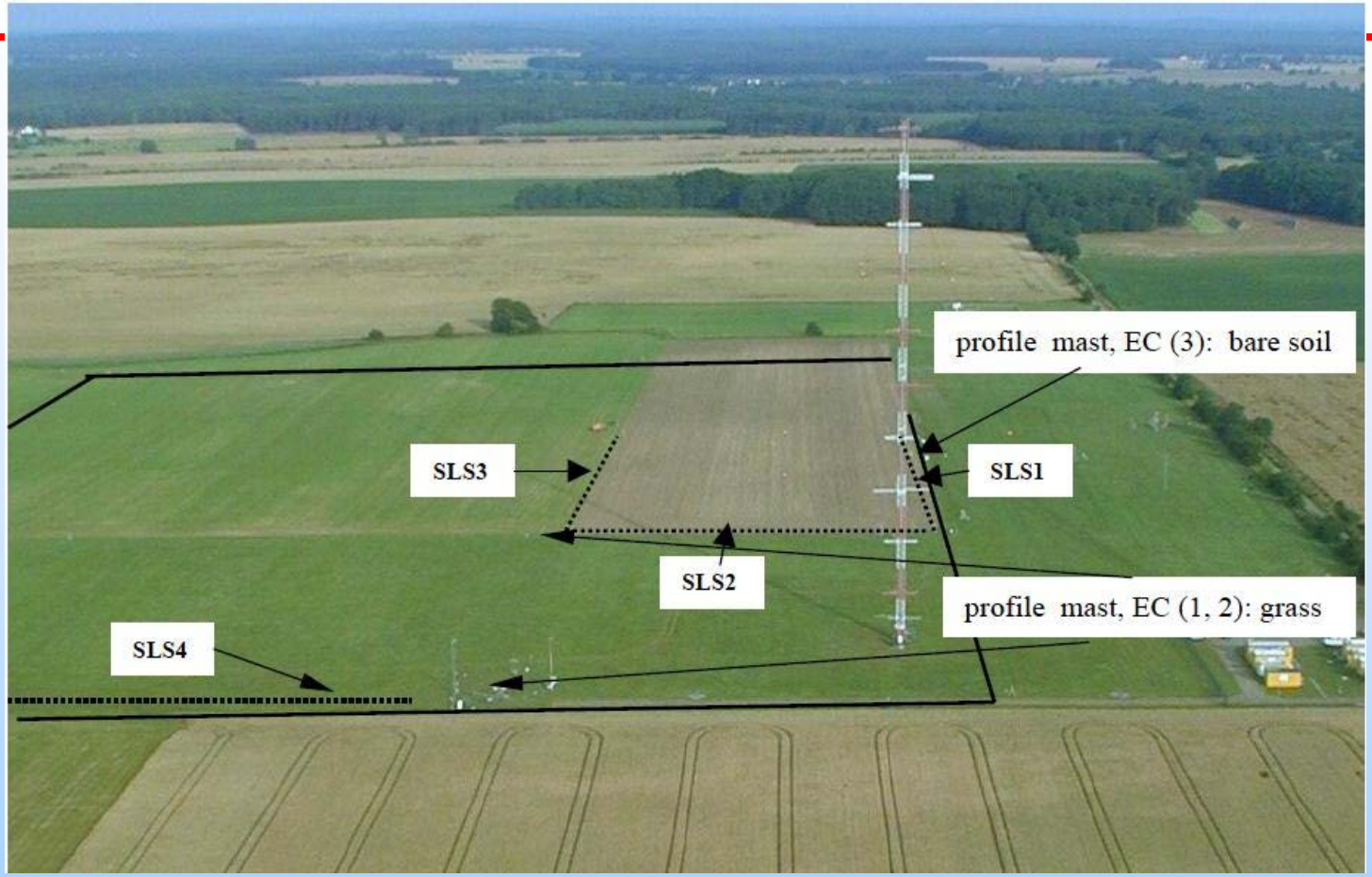

The experimental site consisted of grass and bare soil. The main goal of the experiment was to study the effects of heterogeneous surface on the turbulent heat exchange and horizontal turbulent fluxes. Numerous meteorological equipment including the tomography array was employed to measure parameters of the atmospheric surface layer.

Tomographic reconstruction with TDSI

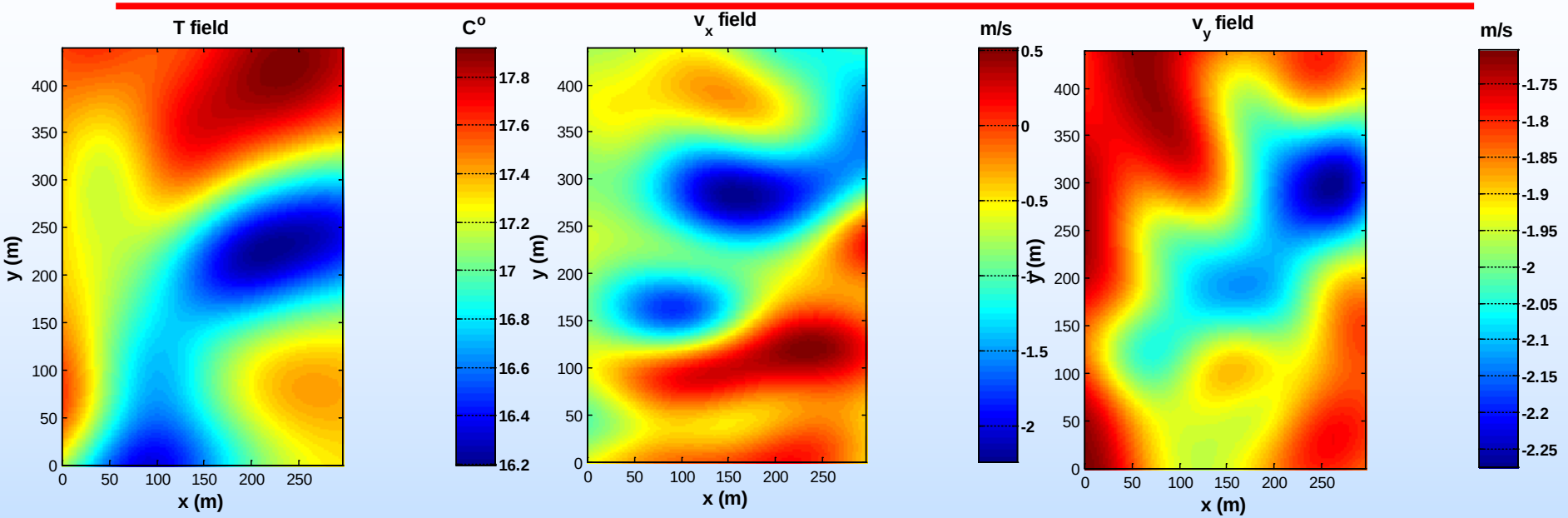

Shown are the temperature and two velocity components reconstructed with TDSI from the travel times provided to us by the German group. Results correspond to 5:30 am on 6 July 2002. Three sets of the travel times were used in TDSI. Expected RMSE in the reconstruction are 0.36 C, 0.35 m/s, and 0.25 m/s. The reconstruction is less detailed than that for the BAO tomography array due to a larger size of the array and less frequent measurements of the travel times. Warm and cold temperature eddies, and fast and slow velocity eddies are seen clearly. The reconstructed values of temperature (at a different time) agree very well with those measured in situ:

In situ, T = 16.24 C; TDSI, 16.14 C. x = 28 m, y = 138 m.

In situ, T = 15.78 C; TDSI, 15.77 C. x = 182 m, y = 143 m.

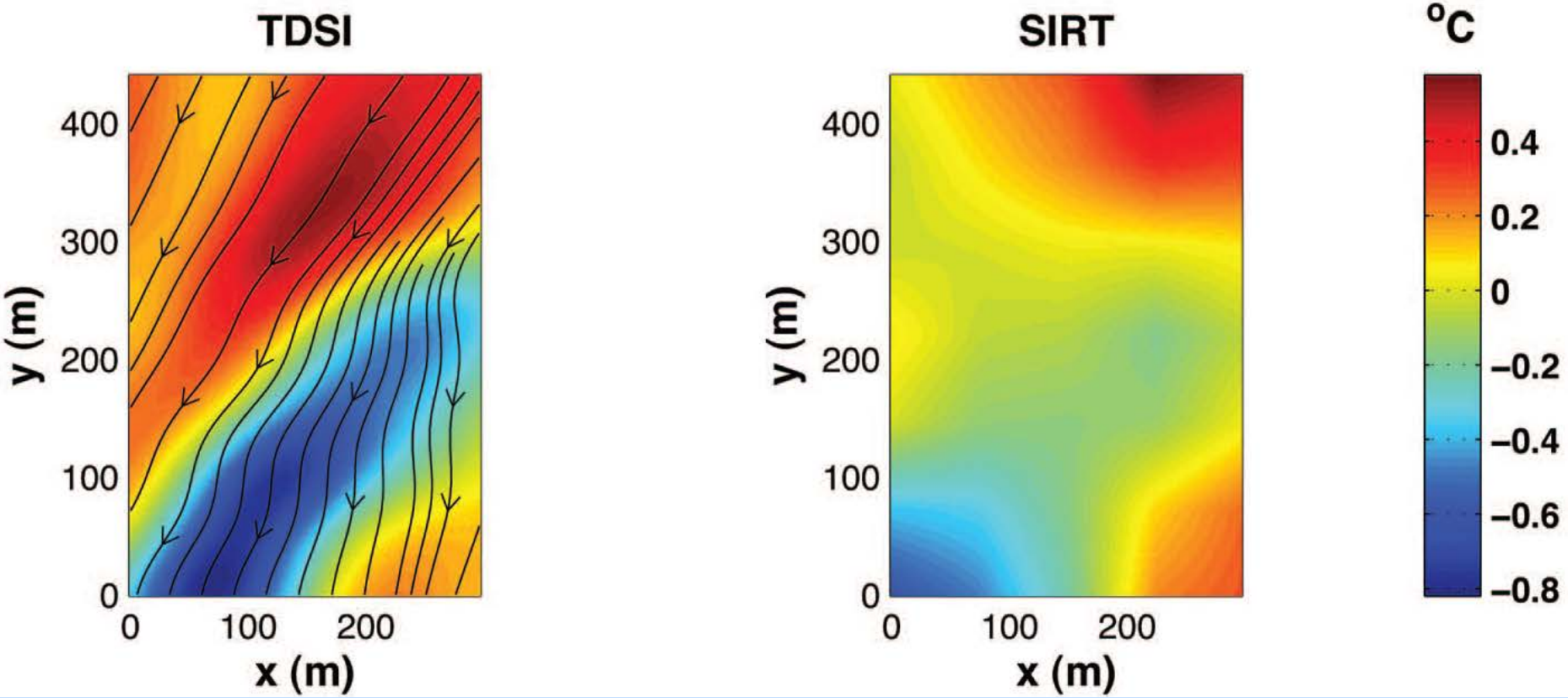

(Left) Temperature field reconstructed with TDSI and averaged over 10 min. Arrows indicate the direction of the averaged wind velocity. Due to heterogeneity of the ground, the temperature has a spatial variation of about 1 C.
(Right) Temperature field reconstructed with an algebraic reconstruction (specifically, Simultaneous Iterative Reconstruction Technique or SIRT). TDSI provides much more detailed reconstruction than SIRT does.

Tomography experiment in a large tank

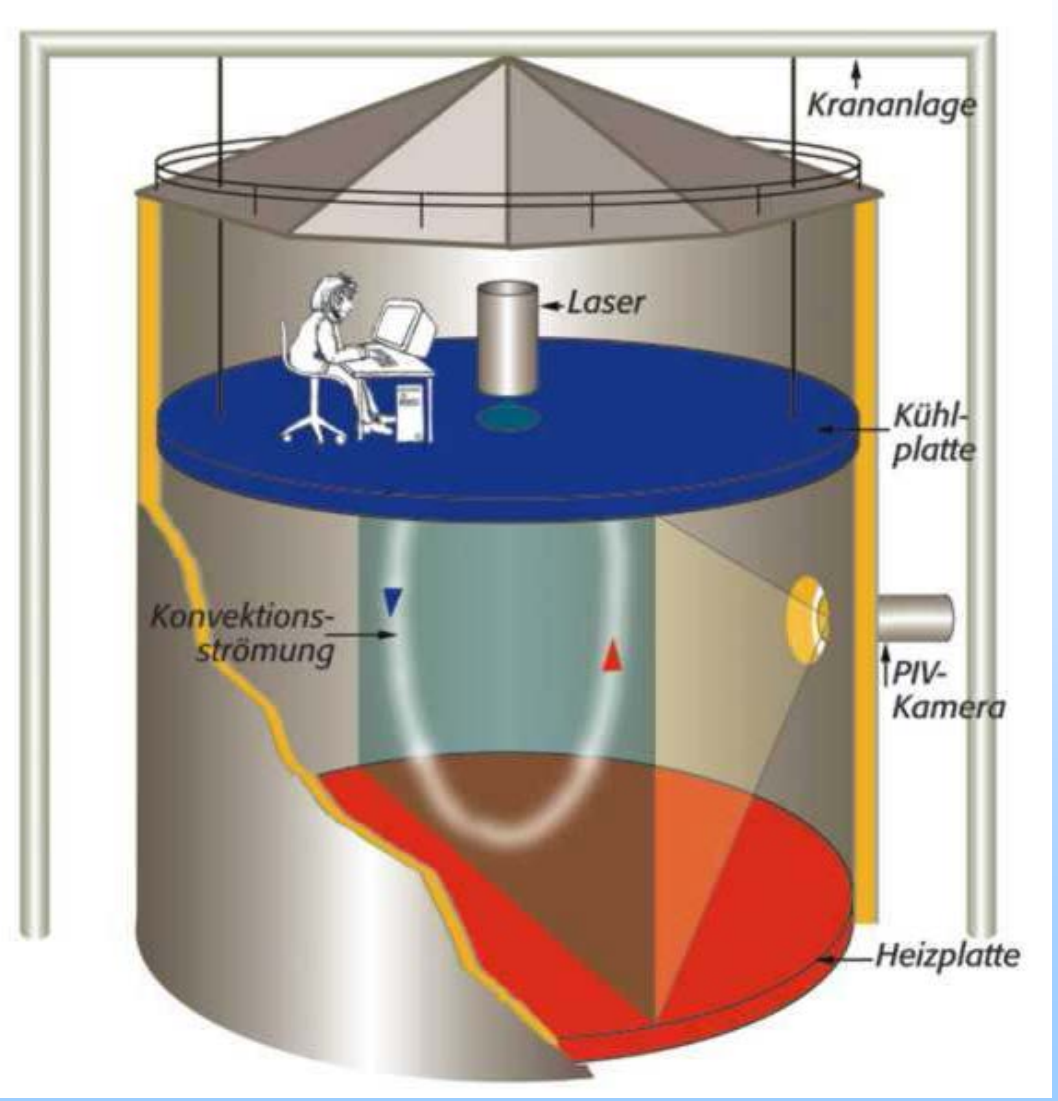

The German group also built a smaller version of the tomography array for indoor applications.

The array was placed between horizontally located heating and cooling plates in a large tank in Ilmenau, Germany to study convection.

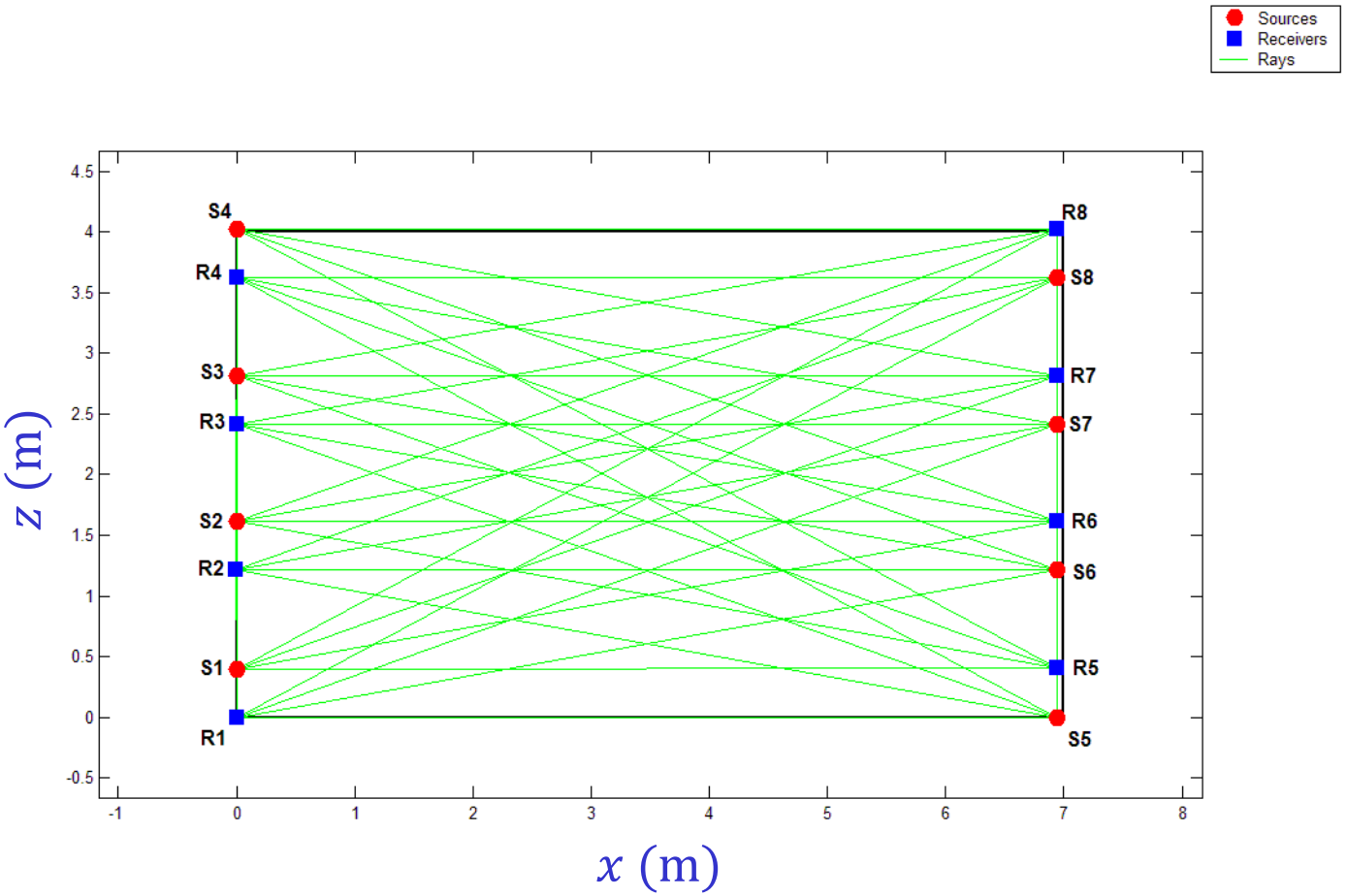

Shown is the schematic of the tomography array with 8 speakers and 8 microphones located in a vertical plane. The size of the array is 7 m x 4 m. Travel times were measured every 20 s.

Reconstruction of the temperature and velocity fields

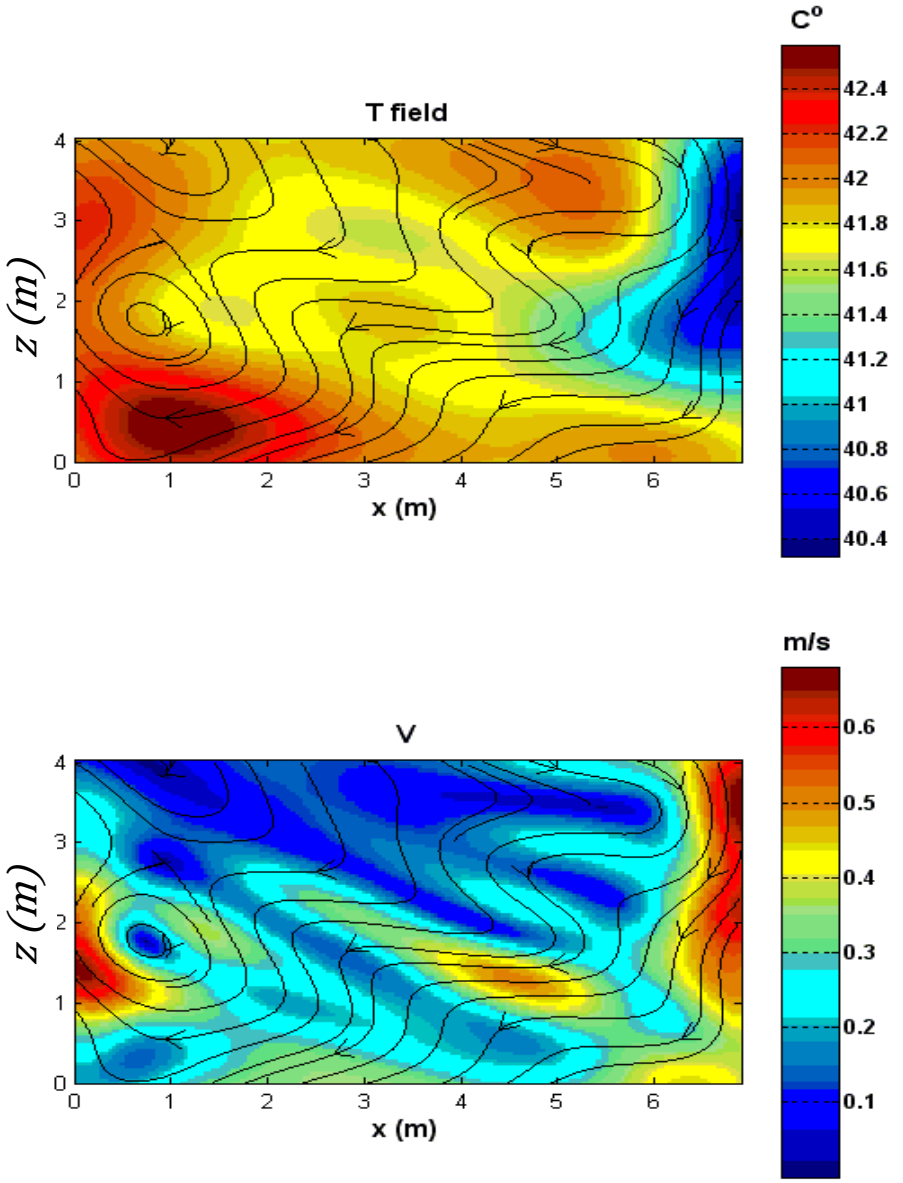

The temperature and the magnitude of the velocity were reconstructed with TDSI from the travel times provided to us by the German group. Five consecutive sets of the travel times were used. The arrows indicate the direction of the velocity. The array was located in the place where the velocity was toward the heating plate.

The temperature varies between 42.6 C at the heating plate and 40 C at the cooling plate. The medium velocity is less than 0.65 m/s which is typical for convection.

The RMSEs in reconstruction are 0.07 C and 0.05 m/s, and are slightly smaller than those for the BAO tomography array due to the smaller size of the array.

Acoustic tomography of the ABL with UAVs

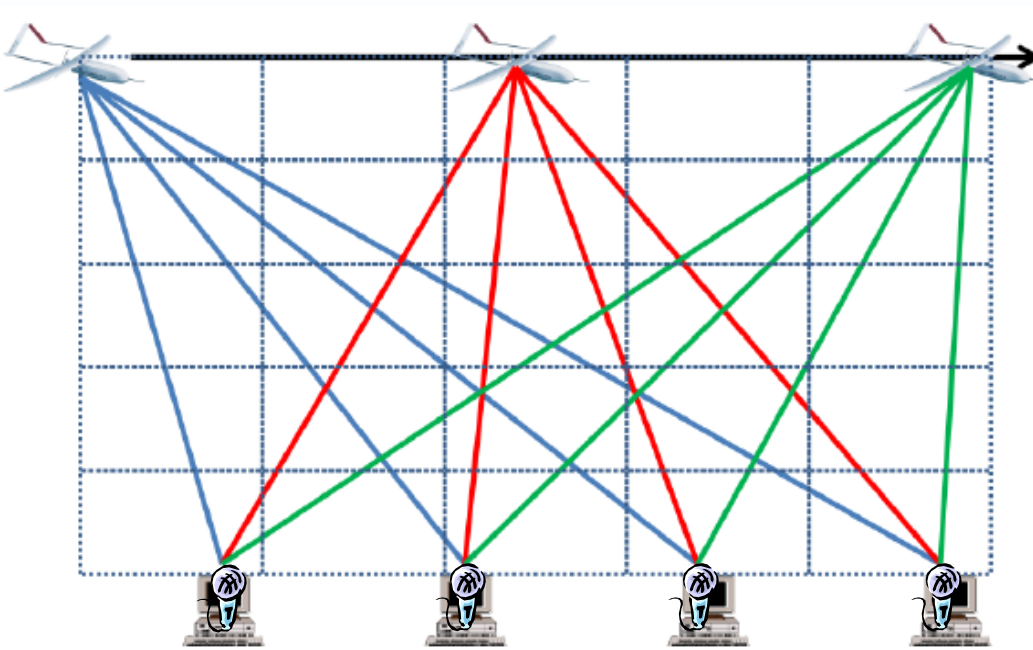

Figure 1: Graphical Depiction of UAV-Based Tomography Concept

Finn and Rogers from the University of South Australia used a small UAV, Aerosonde, to fly at the height of several hundred meters above the ground. It is famous as the first UAV to fly across the Atlantic and in a category 1 cyclone. Propeller noise of the UAV was recorder by microphones on the ground. Using a very elaborate signal processing technique, the travel times of sound propagation from each UAV location to the microphones were determined. The forward problem is similar to that in the BAO tomography array. The reconstruction of the temperature and wind velocity fields is done with a basis function approach. In this approach, the T and v fields are approximated by given functions (e.g., Gaussian envelopes) with parameters to be determined.

Reconstruction of the temperature and wind velocity fields

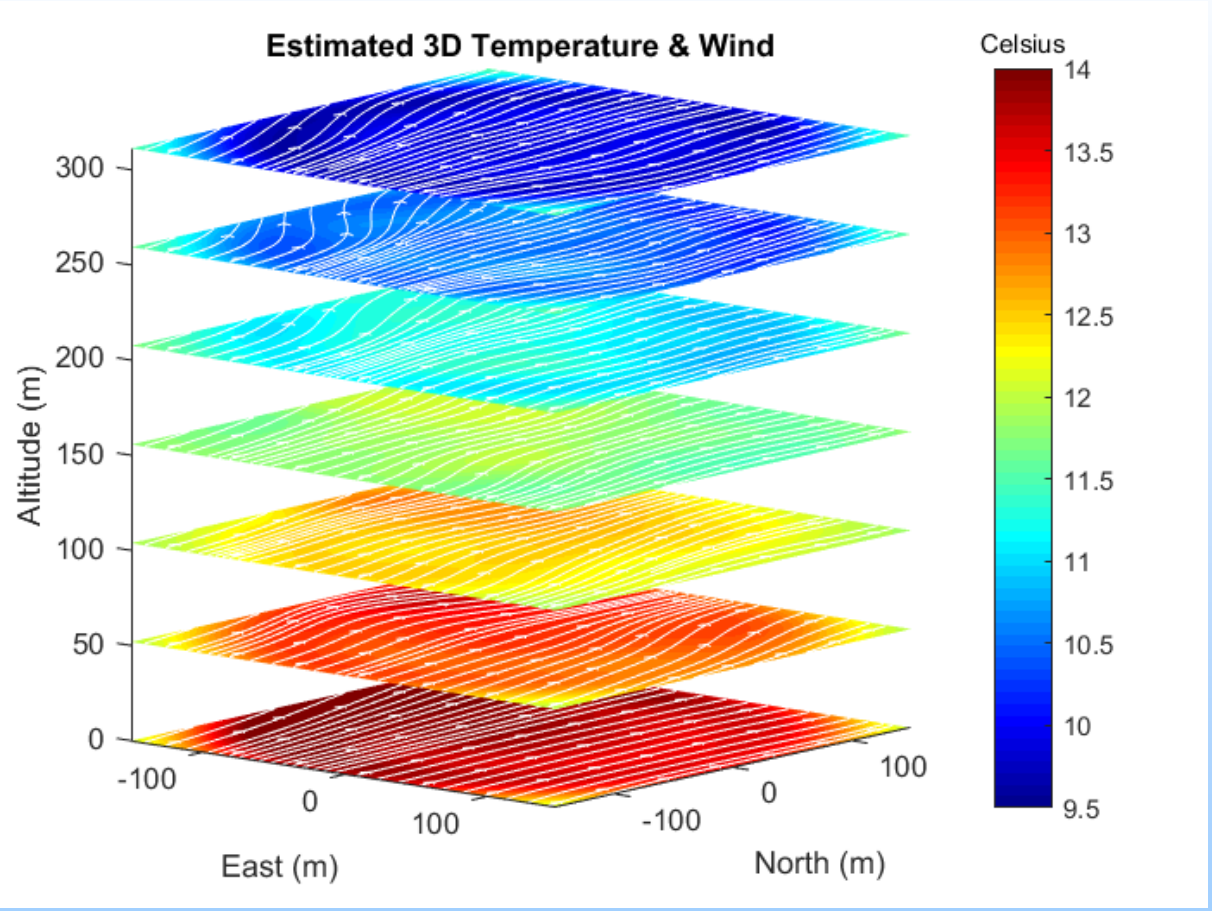

Shown are the reconstructed 3D temperature (colors) and wind velocity (small arrows) fields in a cube with the side length 300 m. The temperature decreases with height by about 5 deg C. The reconstructed temperature field is not very detailed. This is typical for solutions of overdetermined invers problems in ATA such as a basis function approach.

The UAV based ATA can perhaps be improved by using TDSI.

Acoustic tomography of the troposphere

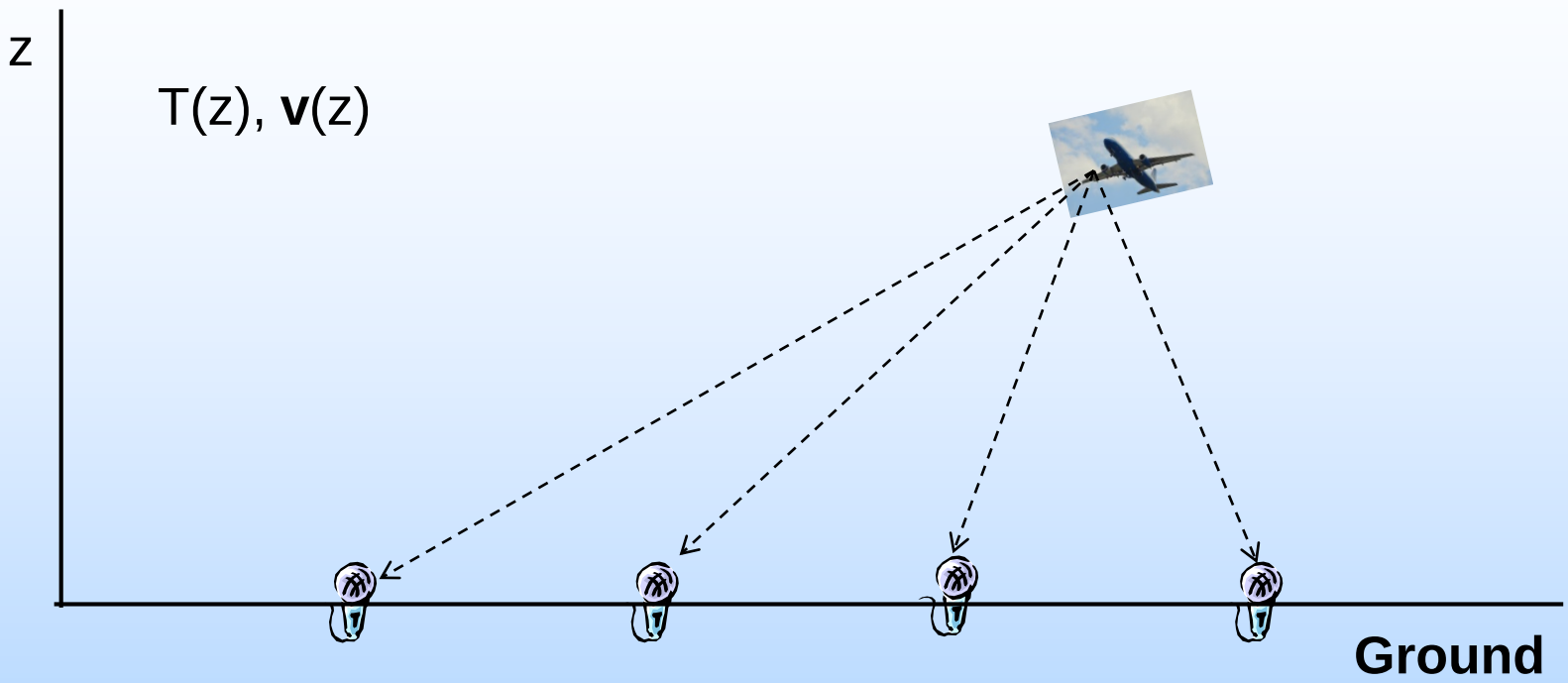

A similar idea was suggested earlier by Wilson et al. (2001). Microphones can be placed on the ground near airports and measure signals from ascending and descending airplanes. By cross-correlating signals at the microphones, the difference in the travel times of sound propagation from an airplane to the microphones can be determined. Then, the vertical profiles of temperature and wind velocity can be reconstructed. This seems as a very inexpensive technique for measuring the vertical profiles. Here, the forward problem is formulated for the vertically stratified atmosphere. The inverse problem can be solved in an analytical form or with a least square estimation.

Acoustic tomography of the upper atmosphere

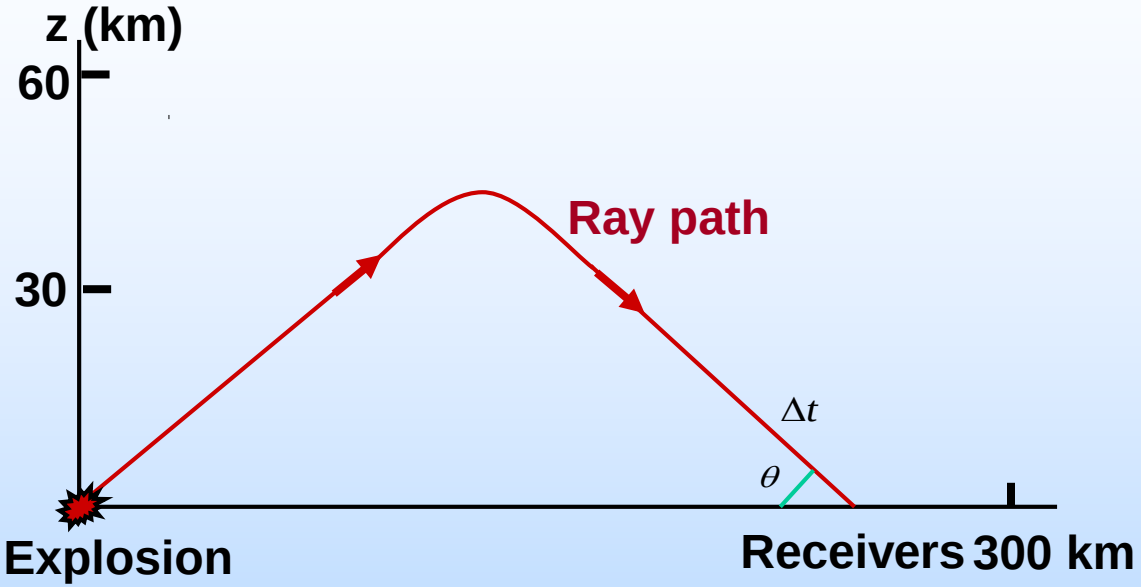

Between the 1900's and 1930's, upper tropospheric and stratospheric wind and temperature profiles were deduced by measuring the travel of sound propagation from large explosions on the ground to receivers also located on the ground. The angles of arrival were also measured.

This technique can be termed as the first acoustic tomography of the atmosphere. The forward problem assumes a vertically stratified atmosphere. Solution of the inverse problem provides the effective sound speed $c_{\text{eff}}(z) = c(z) + v_x(z)$ at the height z of the turning point. Similar remote sensing can be done now with the global infrasound network consisting of several dozens stations of IMS to detect nuclear explosions.

Sonic anemometer as a small tomography array

CSAT3 Sonic anemometer

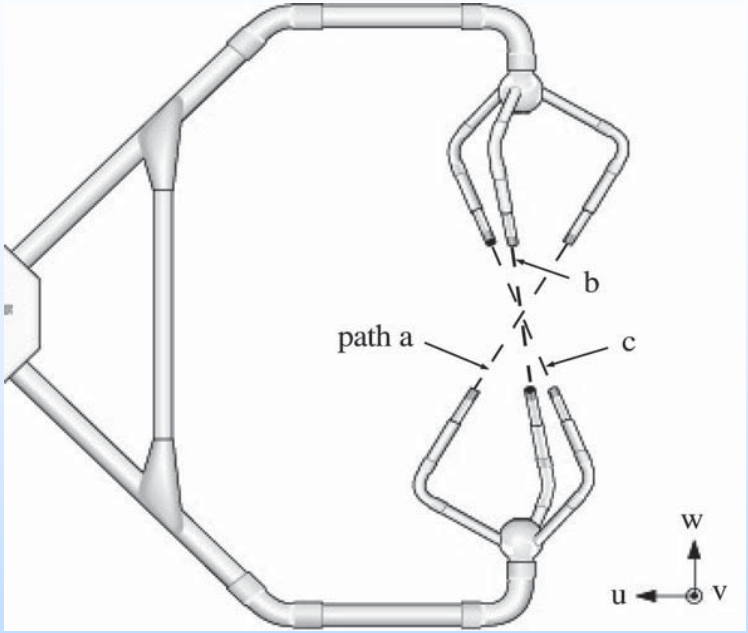

Suggested modification of a sonic

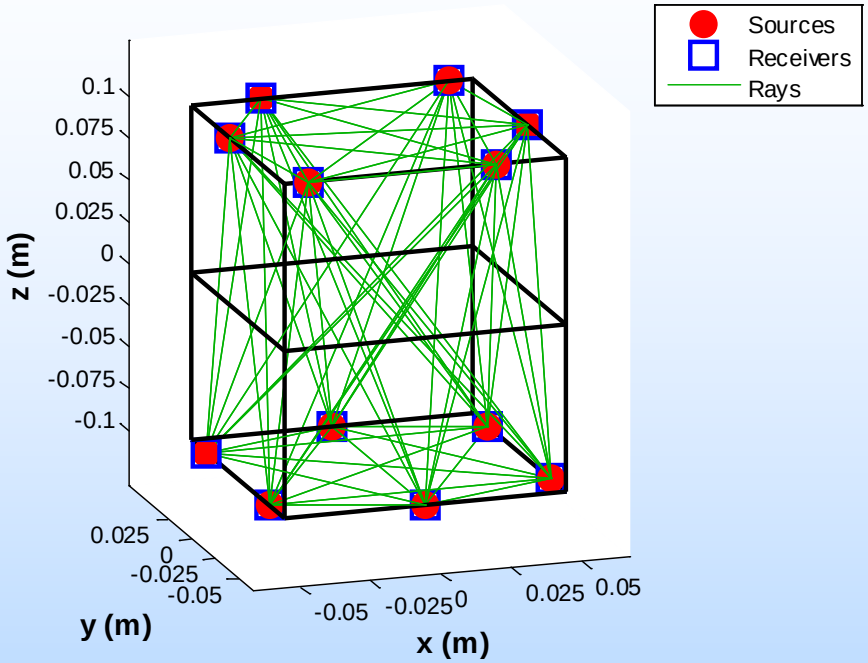

Sonic anemometers are robust instruments for measurements of temperature and wind velocity. Due to concerns about flow distortion, the transducers of a sonic are located at a distance of about 0.2 m thus enabling only path-averaged measurements. Several important applications in boundary-layer physics and turbulence theory require analysis of turbulent fields at smaller scales. To increase the spatial resolution of a sonic anemometer, we suggest considering it as a small acoustic tomography array (Vecherin et al. 2013). A particular modification of the sonic is shown in the right plot. There are 6 transducers at the upper and lower levels. They work as a small tomography array. The forward and inverse problems are formulated similarly to the BAO tomography array, except that this is a 3D acoustic tomography.

Temperature and velocity fields in numerical simulations

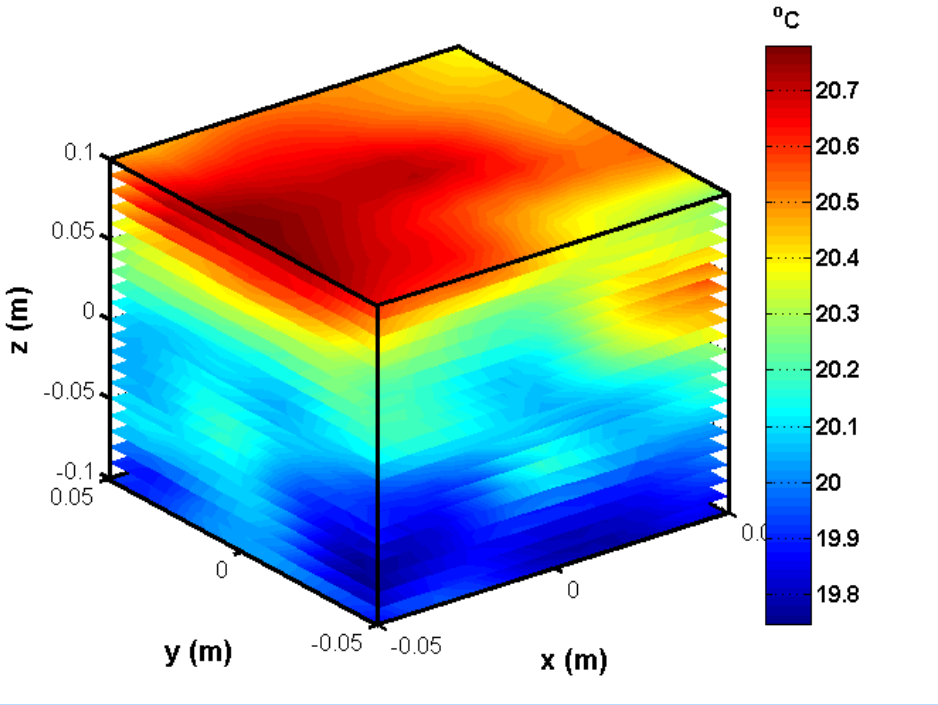

Temperature

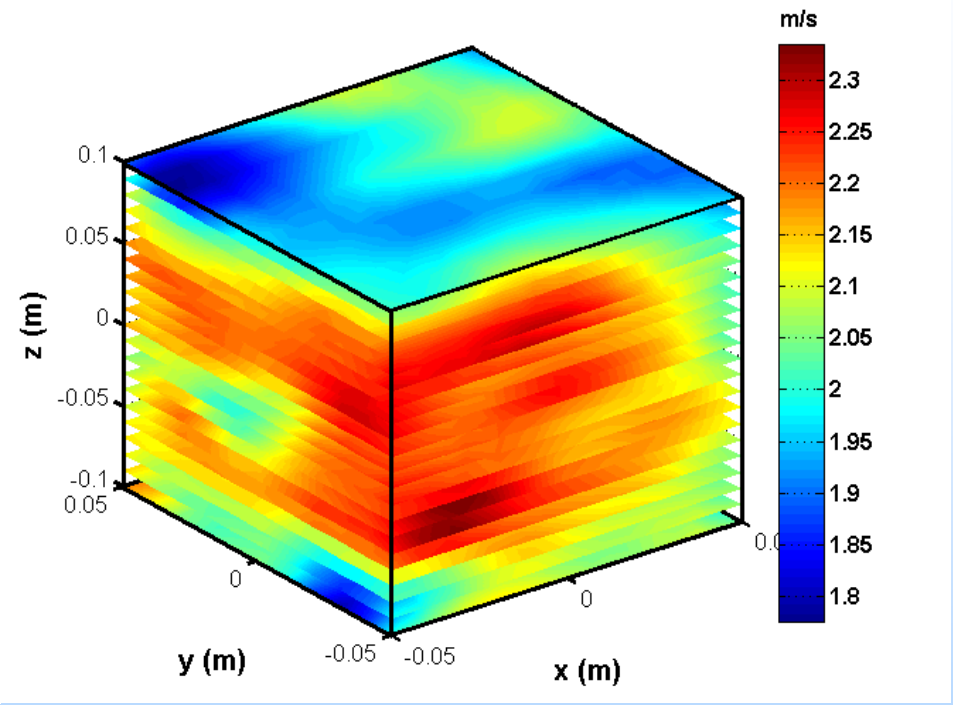

The x-component of velocity

In numerical simulations of the sonic anemometer as a small acoustic tomography array, temperature and velocity fields were modeled with quasi-wavelets (QW), Wilson et al. (2009), Ostashev and Wilson (2015). Using QW fields moving through the sonic, the travel times of sound propagation between 12 transducers were calculated. TDSI was used to reconstruct the temperature and velocity fields.

Results of numerical simulations

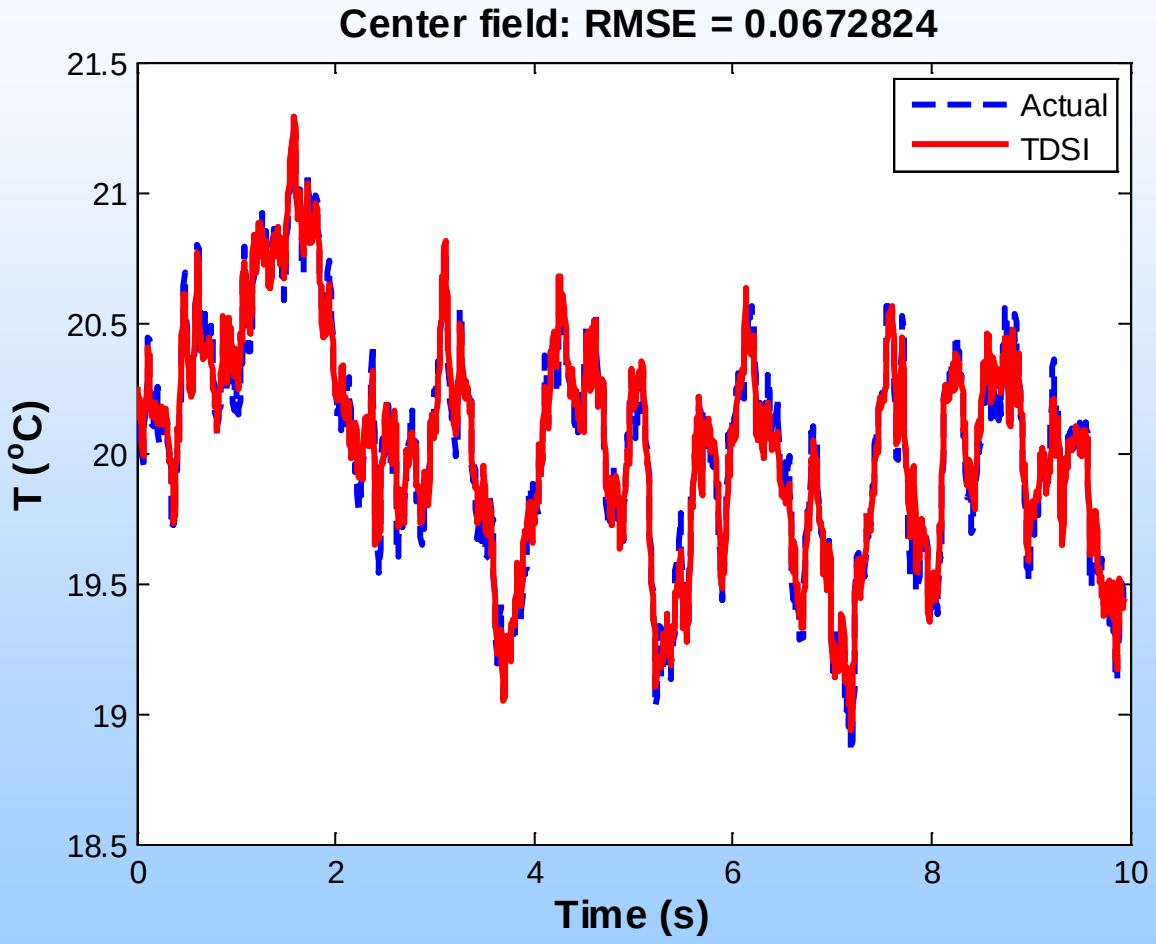

The blue line corresponds to the actual temperature in the center of the sonic anemometer as a small acoustic tomography array. The red line corresponds to that reconstructed with TDSI. The agreement between the actual and reconstructed temperature is very good.

Numerical simulations of a sonic and a sonic as an acoustic tomography array

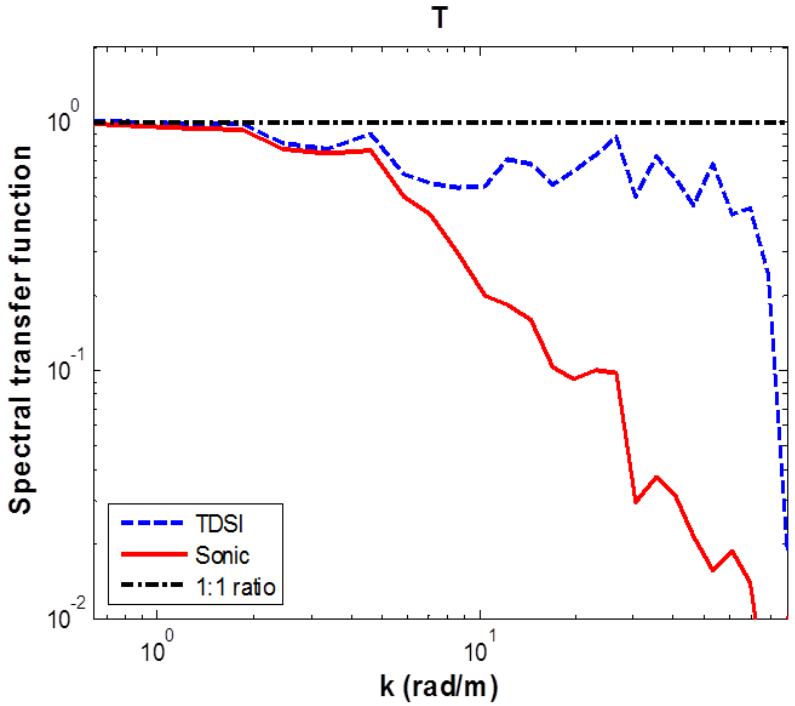

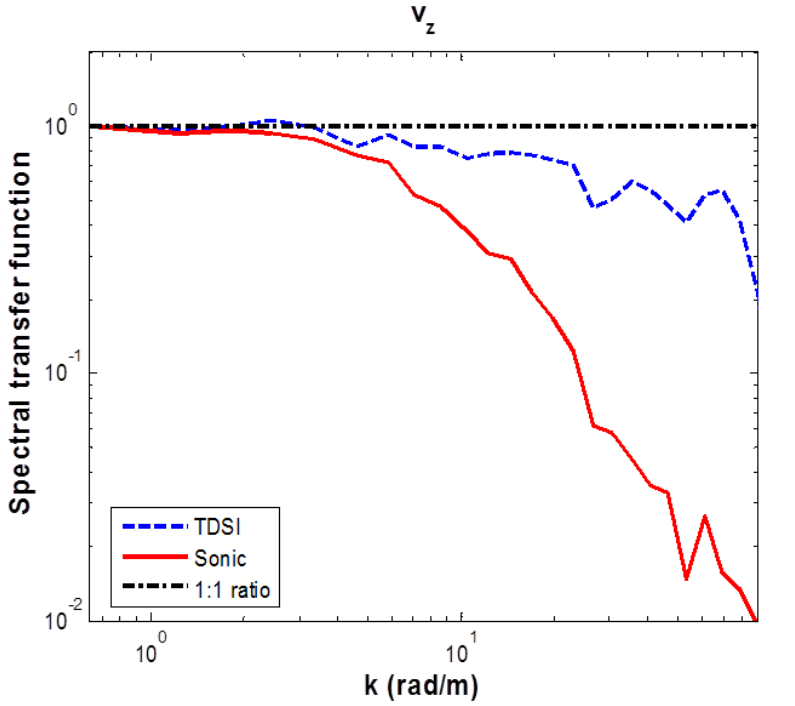

The spectral transfer function is the ratio of the power spectrum of temperature/velocity fluctuations obtained in numerical simulations of a sonic or a sonic as a tomography array and the power spectrum of temperature/velocity fluctuations in the turbulent field moving through the sonic. Solid red lines correspond to numerical simulations of the sonic, while dashed blue lines correspond to the sonic as a tomography array. For a good reconstruction of temperature and velocity, the spectral transfer functions should be close to one. The spectral transfer functions for the sonic drop at much smaller turbulence wavenumbers than those for the sonic as a tomography array. The sonic anemometer as a tomography array enables to increase the spatial resolution by a factor of 10.

6. Conclusions

1. Acoustic tomography of the atmosphere can be done at different scales ranging from a size of a sonic anemometer to the thermospheric heights (about 100 km).

2. By regarding a sonic anemometer as a small acoustic tomography array and applying appropriate inverse algorithms, spatial resolution in reconstruction of the temperature and velocity fields can be increased by a factor of 10 and new atmospheric quantities can be measured. This is important for studies of small-scale turbulence.

3. In the ASL, acoustic tomography is a unique remote sensing technique for simultaneous measurements of the temperature and velocity fields. Acoustic tomography can be used for remote sensing of wind turbine wakes.

4. In the troposphere, acoustic tomography can significantly reduce the cost of remote sensing of the vertical profiles of temperature and wind velocity. Acoustic tomography with UAVs has been demonstrated.

5. Acoustic tomography can also be used to monitor other flows such as those in a wind tunnel.

7. References

Book chapters and journal reviews:

V. E. Ostashev and D. K. Wilson, *Acoustics in Moving Inhomogeneous Media, Second Edition* (CRC Press, 2015), Chapter 3.
V. E. Ostashev, S. N. Vecherin, D. K. Wilson, A. Ziemann, and G. H. Goedecke, “Recent progress in acoustic travel-time tomography of the atmospheric surface layer,” Meteorologische Zeitschrift 18 (2), 125-133 (2009).
D. K. Wilson, A. Ziemann, V. Ostashev, and A. Voronovich, “An overview of acoustic travel-time tomography in the atmosphere and its potential applications,” Acustica-acta acustica 87 (2001).

Selected publications:

S. N. Vecherin, V. E. Ostashev, and D. K.Wilson, “Assessment of systematic errors in acoustic tomography of the atmosphere,” J. Acoust. Soc. Am. 134 (3), 1802-1813 (2013).
S. N. Vecherin, V. E. Ostashev, D. K. Wilson, C. W. Fairall, and L. Bariteau, “Sonic anemometer as a small acoustic tomography array,” Boundary Layer Meteorology 149 (2) 165-178 (2013).
S. N. Vecherin, V. E. Ostashev, and D. K. Wilson, “Three-dimensional acoustic travel-time tomography of the atmosphere,” Acustica-acta acustica 94 (3), 349-358 (2008).

References

S. N. Vecherin, V. E. Ostashev, D. K. Wilson, and A. Ziemann, “Time-dependent stochastic inversion in acoustic tomography of the atmosphere with reciprocal transmission,” Meas. Sci. Technol. 19 (2008).

S. N. Vecherin, V. E. Ostashev, A. Ziemann, D. K. Wilson, K. Arnold, and M. Barth, “Tomographic reconstruction of atmospheric turbulence with the use of time-dependent stochastic inversion,” J. Acoust. Soc. Am. 122 (3), 1416-1425 (2007).

S. N. Vecherin, V. E. Ostashev, G. H. Goedecke, D. K. Wilson, and A. G. Voronovich, “Time dependent stochastic inversion in acoustic travel-time tomography of the atmosphere,” J. Acoust. Soc. Am. 119 (5), 2579-2588 (2006).

S. Kolouri, M. R. Azimi-Sadjadi, and A. Ziemann, “A statistical-based approach for acoustic tomography of the atmosphere,” J. Acoust. Soc. Am. 135 (1), 104-114 (2014).

A. Raabe, K. Arnold, A. Ziemann, M. Schroter, S. Raasch, J. Bange, P. Zittel, Th. Spiess, Th. Foken, M. Gockede, F. Beyrich, J-P. Leps, “STINHO - STructure of turbulent transport under INHOmogeneous conditions - the micro-alpha scale field experiment and LES modeling,” Meteorol. Z. 14, 315-327 (2005).

K. Arnold, A. Ziemann, A. Raabe, G. Spindler, “Acoustic tomography and conventional meteorological measurements over heterogeneous surfaces,” Meteor. Atmos. Phys. 85, 175-186 (2004).

S. Weinbrect, S. Raasch, A. Ziemann, K. Arnold, A. Raabe, “Comparison of large-eddy simulation data with spatially averaged measurements obtained by acoustic tomography – presuppositions and first results,” Boundary Layer Meteorology 111, 441-465 (2004).

References

A. Ziemann, K. Arnold, A. Raabe, “Acoustic tomography as a remote sensing method to investigate the near surface atmospheric boundary layer in comparison with in sit measurements,” J. Atmos. Oceanic Technol. 19, 1208-1215 (2002).

A. Ziemann, K. Arnold, A. Raabe, “Acoustic tomography as a method to identify small-scale land surface characteristics,” Acust. Acta Acust. 87, 731-737 (2001).

A. Finn and K. Rogers, “The Feasibility of Unmanned Aerial Vehicle-Based Acoustic Atmospheric Tomography,” J. Acoust. Soc. Am. 138 (2), 874-889 (2015).

K. J. Rogers and A. Finn, “Three-Dimensional UAV-Based Atmospheric Tomography,” J. Atmos. Oceanic Techn. 30 (2), 336-344 (2013).

K. Rogers and A. Finn, “3D Acoustic Atmospheric Tomography,” Proc. SPIE Conf. Rem. Sens., 2014 (International Society for Optics and Photonics, 2014).

D. K. Wilson and D. W. Thomson, “Acoustic tomographic monitoring of the atmospheric surface layer,” J. Atmos. Ocean. Tech. **11**, 751–769 (1994).

I. Jovanovic, L. Sbaiz, and M. Vetterli. “Acoustic tomography for scalar and vector fields: theory and application to temperature and wind estimation. J. Atmos. Ocean. Tech., 26, 1475-1492 (2009).